

The hot core towards the intermediate mass protostar NGC 7129 FIRS 2

Chemical similarities with Orion KL[★]

A. Fuente¹, J. Cernicharo², P. Caselli³, C. M^cCoey⁴, D. Johnstone^{5,6,7}, M. Fich⁴, T. van Kempen⁸, Aina Palau⁹, U.A. Yıldız¹⁰, B. Tercero², and A. López²

¹ Observatorio Astronómico Nacional (OAN,IGN), Apdo 112, E-28803 Alcalá de Henares (Spain) e-mail: a.fuente@oan.es

² Instituto de Ciencia de Materiales de Madrid (ICMM) C/Sor Juana Inés de la Cruz N3, Cantoblanco, 28049 Madrid, Spain

³ Max Planck Institute for Extraterrestrial Physics, Postfach 1312, 85741 Garching, Germany

⁴ Department of Physics and Astronomy, University of Waterloo, Waterloo, Ontario, N2L 3G1, Canada

⁵ Department of Physics & Astronomy, University of Victoria, Victoria, BC, V8P 1A1, Canada

⁶ National Research Council of Canada, Herzberg Institute of Astrophysics, 5071 West Saanich Road, Victoria, BC, V9E 2E7, Canada

⁷ Joint Astronomy Centre, 660 North A'ohoku Place, University Park, Hilo, HI 96720, USA

⁸ Leiden Observatory, Leiden University, P.O. Box 9513, 2300 RA Leiden, Netherlands

⁹ Centro de Radioastronomía y Astrofísica, Universidad Nacional Autónoma de México, P.O. Box 3-72, 58090 Morelia, Michoacán, México

¹⁰ Jet Propulsion Laboratory, California Institute of Technology, 4800 Oak Grove Drive, Pasadena CA, 91109, USA

Preprint online version: November 8, 2021

ABSTRACT

Context. This paper is dedicated to the study of the chemistry of the intermediate-mass (IM) hot core NGC 7129 FIRS 2, probably the most compact warm core found in the 2 to 8 M_{\odot} stellar mass range.

Aims. Our aim is to determine the chemical composition of the IM hot core NGC 7129 FIRS 2, providing new insights on the chemistry of hot cores in a more general context.

Methods. NGC 7129 FIRS 2 (hereafter, FIRS 2) is located at a distance of 1250 pc and high spatial resolution observations are required to resolve the hot core at its center. We present a molecular survey from 218200 MHz to 221800 MHz carried out with the IRAM Plateau de Bure Interferometer (PdBI). These observations were complemented with a long integration single-dish spectrum taken with the IRAM 30m telescope in Pico de Veleta (Spain). We used a Local Thermodynamic Equilibrium (LTE) single temperature code to model the whole dataset.

Results. The interferometric spectrum is crowded with a total of ≈ 300 lines from which a few dozens remain unidentified yet. The spectrum has been modeled with a total of 20 species and their isomers, isotopologues and deuterated compounds. Complex molecules like methyl formate (CH_3OCHO), ethanol ($\text{CH}_3\text{CH}_2\text{OH}$), glycolaldehyde (CH_2OHCHO), acetone (CH_3COCH_3), dimethyl ether (CH_3OCH_3), ethyl cyanide ($\text{CH}_3\text{CH}_2\text{CN}$) and the G conformer of ethylene glycol (aGg'-(CH_2OH)₂) are among the detected species. The detection of vibrationally excited lines of CH_3CN , CH_3OCHO , CH_3OH , OCS, HC_3N and CH_3CHO proves the existence of gas and dust at high temperatures. In fact, the gas kinetic temperature estimated from the vibrational lines of CH_3CN , $\sim 405^{+100}_{-67}$ K, is similar to that measured in massive hot cores. Our data allow an extensive comparison of the chemistry in FIRS 2 and the Orion hot core.

Conclusions. We find a quite similar chemistry in FIRS 2 and Orion. Most of the studied fractional molecular abundances agree within a factor of 5. Larger differences are only found for the deuterated compounds D_2CO and CH_2DOH and a few molecules ($\text{CH}_3\text{CH}_2\text{CN}$, SO_2 , HNCO and CH_3CHO). Since the physical conditions are similar in both hot cores, only different initial conditions (warmer pre-collapse and collapse phase in the case of Orion) and/or different crossing time of the gas in the hot core can explain this behavior. We discuss these two scenarios.

Key words. astrochemistry – stars:formation – ISM: molecules – ISM: individual (NGC 7129 FIRS 2)

1. Introduction

Intermediate-mass young stellar objects (IMs) are the precursors of stars in the 2–8 M_{\odot} mass range (Herbig Ae/Be stars). They share some characteristics with massive young stellar objects (clustering, PDR) but they are more common than the more massive stars and therefore they can be found closer to

the Sun ($d < 1$ kpc), which allows determination of the physical and chemical structure of their envelopes at similar spatial scales as can be done for low mass protostars. From a chemical point of view, IMs are interesting because they constitute the link between the low-mass and high-mass ranges, covering an intermediate range of luminosities, densities and temperatures.

Hot molecular cores are compact (< 0.05 pc) objects with high temperatures (> 100 K) and densities ($n(\text{H}_2) > 10^6 \text{ cm}^{-3}$), which are characterized by a very rich chemistry of complex organic molecules (COMs). In fact, the prototype of massive

Based on observations carried out with the IRAM Plateau de Bure Interferometer. IRAM is supported by INSU/CNRS (France), MPG (Germany), and IGN (Spain).

hot core, that associated with Orion KL, hosts one of the richest molecular chemistry observed in the interstellar medium (Blake et al. 1987; Beuther et al. 2005, 2006; Tercero et al. 2010, 2011, 2013; Motiyenko et al. 2012, Cernicharo et al. 2013). COMs have also been detected, coming from the inner regions of a few low-mass protostars, the so called hot corinos (IRAS 16293-2422: Cazaux et al. 2003, Bottinelli et al. 2004a, Pineda et al. 2012; NGC 1333 IRAS 2A: Jørgensen et al. 2005, 2007; NGC1333-IRAS 4AB: Bottinelli et al. 2004b, Bottinelli et al. 2007). These regions have smaller sizes (~ 150 AU) and lower temperatures (~ 100 K). Although high sensitivity interferometric data on hot cores and corinos are still scarce and the comparison is difficult, there is some general consensus that hot corinos are richer in O-bearing molecules like CH_3OCHO , CH_3CHO , CH_3OCH_3 or HCOOH , and poorer in N-bearing compounds. Furthermore, large abundances of deuterated molecules and large deuterium fractions are only associated with hot corinos (Vastel et al. 2003; Parise et al. 2004; Demyk et al. 2010).

A handful of well studied hot cores exist in the IM range: NGC 7129 FIRS 2 (Fuente et al. 2005a, hereafter FU05), IC 1396 N (Neri et al. 2007, Fuente et al. 2009), IRAS 22198+6336 (Sánchez-Monge et al. 2010, Palau et al. 2011), AFGL 5142 (Palau et al., 2011). The sizes of these IM hot cores range from ~ 130 AU (IRAS 22198) to ~ 900 AU (NGC 7129) and their chemistries present some differences. FU05 proposed that IM hot cores, like hot corinos, are richer in H_2CO and HCOOH relative to CH_3OH than massive hot cores, and they did not find any variation in the $\text{CH}_3\text{CN}/\text{CH}_3\text{OH}$ abundance ratio across the stellar range. Palau et al. (2011) studied the chemistry of IRAS 22198+6336 and AFGL 5142 and concluded that these IM hot cores are richer in oxygenated molecules with two or more $\text{CH}_2/3$ -groups than hot corinos but poorer in N-bearing molecules than massive hot cores. As yet, the number of studied objects is very low and the derived column densities have large uncertainties.

In this paper, we present a 4 GHz interferometric frequency survey towards the hot core NGC 7129 FIRS 2 (hereafter, FIRS 2) that, with a luminosity of $\sim 500 L_\odot$, lies near the middle of the IM luminosity range. FIRS 2 is a prototypical young IM protostar, it is associated with energetic outflows (Fuente et al. 2001) and presents clear signs of CO depletion and enhanced deuterium fractionation when observed with single-dish telescopes (scales of ~ 10000 AU) (Fuente et al. 2005b; Alonso-Albi et al. 2010). It is located at a distance of 1250 ± 50 pc from the Sun (Shevchenko & Yakubov 1989) and FU05 detected a compact hot core at its center. FIRS 2 was observed with Herschel within the Water In Star-forming regions (WISH) key program (van Dishoeck et al. 2011) and it is one of the best known IM protostars with a quite complete set of data at both millimeter and far-IR wavelengths (Johnstone et al. 2010, Fich et al. 2010, Fuente et al. 2012). This source and IRAS 22198+6336 are the only hot cores without clear signs of clustering which suggests that their luminosity could come from a single binary system (Palau et al. 2013).

2. Observations

The interferometric observations were carried out with the Plateau de Bure Interferometer (PdBI) in its CD configuration during August and November, 2012. This configuration provided an angular resolution of $1.43'' \times 1.26''$ PA 144° (~ 1870 AU \times 1647 AU at the distance of FIRS 2) at the central frequency. The 1 mm receivers were tuned at 219.360 GHz which allowed the simultaneous imaging of the C^{18}O $2 \rightarrow 1$ and

C^{13}CO $2 \rightarrow 1$ lines, both within the ~ 4 GHz receiver's band. The narrow 40 MHz correlator units were used to sample the C^{18}O and C^{13}CO lines at the high spectral resolution of 40 kHz. The wide band correlator WideX sampled the whole 4 GHz bandwidth with a spectral resolution of ~ 2 MHz. MWC 349 was used as flux calibrator (1.92 Jy) and the rms in each Widex channel, 4–6 mJy/beam (~ 0.058 - 0.087 K).

The interferometric observations were complemented with single-dish observations using the 30m telescope and the same frequency setup. These observations were done in December 2012 and the achieved rms(T_a^*) was ~ 0.012 K (0.09 Jy) in a channel of ~ 1.953 MHz. Therefore, the 30m observations are ~ 15 times less sensitive than the PdBI images. The telescope was pointed towards the phase center of the interferometric observations: $21^{\text{h}}43^{\text{m}}01^{\text{s}}.7$, $+66^\circ 03' 23''.6$ (J2000). Forward and main beam efficiencies are 0.92 and 0.63, respectively. The selected intensity scale is main beam temperature.

This paper is dedicated to the analysis of the chemical complexity revealed by the WideX data towards the mm continuum source.

3. Results

3.1. Continuum maps

The high density of lines detected made it impossible to accurately measure the continuum flux from the low spectral resolution WideX data. Instead, we used the empty emission channels around the C^{18}O and C^{13}CO lines measured at higher spectral resolution using the 40 MHz correlator units to determine the continuum flux. As expected, the continuum flux was slightly different at 219.560 GHz and 220.398 GHz. We derived two continuum maps at 219.560 GHz and 220.299 GHz. Fitting the visibilities we obtained the position of the compact source: $21^{\text{h}}43^{\text{m}}01^{\text{s}}.67$, $+66^\circ 03' 23''.7$, i.e., offset by $-0.17''$ in right ascension from our phase center. The measured fluxes are 0.37(0.01) Jy at 219.560 GHz and 0.38(0.01) at 220.398 GHz, respectively. In FU05, we determined a mm emission spectral index of 2.56 based on the continuum images at 86 GHz and 230 GHz. The new fluxes at 219.6 GHz and 220.4 GHz are consistent with these results taking into account the uncertainty of 10% in the absolute flux calibration.

3.2. Molecular Lines

In Figs. A.1-4 we show the WideX spectra towards the continuum peak. The continuum image at 219.560 GHz was subtracted from the spectral maps before the cleaning process. This subtraction is not perfect since the continuum presents a smooth slope across the observed bandwidth, but it is good enough for our current detection goals.

The spectrum towards the compact source is crowded with lines, typical of those found in massive hot cores. In order to estimate the flux that the interferometer is missing, we compared the PdBI spectrum with that obtained with the 30m telescope. In Table 1 we show the list of all the lines detected with both telescopes and the fraction of flux recovered using the PdBI. Note that only the H_2CO , CH_3OH , SO , C^{18}O and C^{13}CO lines are missing a significant fraction of their fluxes when observed with the PdBI. The emission of OCS , HNCO , CH_3CN and HC_3N comes mainly from the hot core although 20% of the flux of the lowest energy HNCO line is missing. This is also consistent with the spatial distribution as observed with the PdBI. In Fig. 1, we show the integrated intensity images of some of the more intense

Table 2. Results of the rotational diagram analysis¹

Species	T_{rot} (K)	N (cm^{-2})	R^2
HNCO	260^{+4}_{-5}	$1.6^{+0.1}_{-0.1} \times 10^{15}$	0.99
$\text{CH}_3\text{CN } \nu=0^3$	905^{+250}_{-161}	$1.6^{+0.2}_{-0.2} \times 10^{15}$	0.90
$\text{CH}_3\text{CN } \nu_8=1$	405^{+100}_{-67}	$9.4^{+3.1}_{-3.1} \times 10^{14}$	0.81
$\text{CH}_3\text{OCHO } \nu_1=0,1$	265^{+139}_{-69}	$2.8^{+1.9}_{-0.8} \times 10^{16}$	0.60
CH_2DOH	157^{+15}_{-13}	$1.4^{+0.3}_{-0.3} \times 10^{16}$	0.99
$\text{aGg}^7\text{-(CH}_2\text{OH)}_2$	145^{+37}_{-25}	$2.0^{+0.3}_{-0.3} \times 10^{15}$	0.92

¹Beam filling solution. ²Correlation coefficient of the least square fitting. ³This fit was not finally used in the model because the detection of the ¹³C isotopologue showed that the lines are optically thick.

lines. Only ¹³CO, C¹⁸O and SO present large scale structure. In all the other molecules the emission is point-like at the angular resolution of our observations.

4. Line identification and rotational diagrams

For line identification we used José Cernicharo’s personal catalogue which is included in the radiative transfer and molecular excitation code MADEX (Cernicharo 2012), the JPL (Pickett 1991,1998) and the CDMS (Müller et al. 2001, 2005) catalogues. Our procedure can be summarized as follows: We started with the identification of the lines of the most common species. The rotation temperatures, molecular column densities and source sizes were estimated by fitting the line intensities of the whole family of molecules (all isotopologues) within the program MADEX. In these calculations, we assume Local Thermodynamic Equilibrium, $v_{\text{LSR}} = -10 \text{ km s}^{-1}$, a linewidth of 8 km s^{-1} and a face-on disk as the source morphology. In the case of a good fit, we create a synthesized spectrum using the derived parameters and subtract it from the observations. Then, we go on with line identification in the residual spectrum. Sometimes, especially for the weak lines, the fit was not good enough. In these cases, we did not subtract the synthesized spectrum in order to avoid spurious features and just went on identifying the features in the original spectrum.

The number of parameters that can be determined for each species depends on the number of lines detected. For example, the source size can only be determined when the lines of the main isotopologue are optically thick. In the optically thick case, $T_{\text{B}} \approx \eta_{\text{ff}} \times J_{\nu}(T_{\text{rot}})$, where η_{ff} is the beam filling factor, and $J_{\nu}(T_{\text{rot}}) = h\nu/kT_{\text{rot}} \times (1 - \exp(h\nu/kT_{\text{rot}}))^{-1}$ with T_{rot} , the rotation temperature. Providing that we know T_{rot} , we can estimate the effective size of the emitting region from the line intensities. The emission sizes cannot be constrained if the main isotopologue lines are optically thin.

For the less abundant molecules, the number of detected lines was too low or the line intensities were too uncertain to estimate the rotation temperature. In these cases, a rotation temperature of $\sim 200 \text{ K}$ was assumed and only the molecular column densities are calculated using MADEX. In Sect. 4.1 to 4.19, we give a more detailed description of the fitting for each species and the results of these calculations are shown in Tables 2 and 3.

Frequencies and line identifications are shown in Table A.1. We compare our synthesized spectrum including all species with observations in Figs. A.1-4.

4.1. Methyl cyanide: CH_3CN , $\text{CH}_3^{13}\text{CN}$

Methyl cyanide (CH_3CN) is one of the best thermometers in hot cores. The symmetric rotor presents a K -ladder structure with transitions that are easily thermalized at the densities prevailing in hot cores. Besides, it is well known that this molecule is especially abundant in this kind of regions. We have detected the whole $12_K \rightarrow 11_K$ ladder, from $K=0$ to $K=11$ in the $\nu=0$ ground vibrational state and in the $\nu_8=1$ vibrational level at $E_{\text{vib}}=525.17 \text{ K}$ (see Table A.4). The high number of detected lines would allow us to determine the rotation and vibrational temperature of this molecule providing that the emission is optically thin (see Fig. 2). As discussed below, this is not the case of the $\nu=0$ lines. Instead, we used the $\nu_8=1$ lines to estimate the rotation temperature. Unfortunately, most of the lines are blended or partially blended. This is the cause of the large uncertainties in the integrated intensities shown in Table A.4. All the lines have $T_b > 3\sigma$ but the uncertainty in the linewidth is large for partially blended lines. As a first step we plotted all the detected lines in a rotational diagram and visually check if any of them were clearly above or below the straight line defined by the other points. We removed the line at 221265 MHz that was clearly above the fit and derived $T_{\text{rot}}=405^{+100}_{-67} \text{ K}$ using the rest of the points (the parameters of this fit are shown in Table 2). The fit was good ($R=0.81$) suggesting that the contribution of other species to the measured line integrated intensities were within the errors. To corroborate this assumption, as a second step, we removed the lines that were severely blended (difference in frequency less than 4 MHz) and kept only those that were isolated or partially blended. At the end we had only 8 transitions and derived $T_{\text{rot}}=609^{+357}_{-167} \text{ K}$. The higher rotation temperature was due to the suppression of the lines at 221199, 221394, 221403 and 221422 MHz. The obtained value was still in agreement with our previous fit within the errors. We were worried because the velocity integrated line intensities of the transitions with $E_{\text{rot}} > 400 \text{ K}$ (221059, 221210 MHz) present large uncertainties. In order to check the robustness of our temperature estimate, we make a new least square fitting without these lines. This fit provided a lower limit to the rotation temperature of $T_{\text{rot}}=250^{+110}_{-59} \text{ K}$. Again the value obtained for the rotation temperature is in agreement with that shown in Table 2 within the errors. Therefore, we decided to keep the estimate shown in Table 2 as a good value for the average rotation temperature although we are aware that, more likely, we have strong temperature gradients across the hot core with temperatures varying between $\sim 250 \text{ K}$ and $\sim 600 \text{ K}$.

The results from the $\text{CH}_3\text{CN } \nu=0$ rotational diagram are shown in Table 2. We obtained a higher rotational temperature in $\nu=0$ than in $\nu_8=1$. One could think that the high temperature in the ground vibrational state was an artifact due to the missing flux in the low K components of the $\text{CH}_3\text{CN } 12_K \rightarrow 11_K$ ladder. However, comparison of the interferometric PdBI and single-dish 30m observations showed that the spatial filtering is not important and therefore this possibility was discarded. An alternative explanation is that the ground state vibrational lines are optically thick. The opacity can be derived by comparing the CH_3CN and $\text{CH}_3^{13}\text{CN}$ lines (the lines of the other ¹³C isotopologue ¹³ CH_3CN are outside the observed frequency range). Unfortunately the $\text{CH}_3^{13}\text{CN } 12_0 \rightarrow 11_0$ and $12_1 \rightarrow 11_1$ lines are blended with those of the main isotopologue. The lowest K transition without any obvious contamination is $K=4$ (220571 MHz) where we have a feature with $T_b \sim 0.39 \text{ K}$ (with an uncertainty of 25% because of partial blending with other lines). Comparing with the main isotopologue, we have $I(\text{CH}_3\text{CN } 12_4 \rightarrow 11_4)/I(\text{CH}_3^{13}\text{CN } 12_4 \rightarrow 11_4) \sim 7$, which im-

Table 1. 30m/PdBI lines¹

Line		Freq (MHz)	30m Flux ² (Jy×km s ⁻¹)	PdBI Flux ³ Flux (Jy/beam×km s ⁻¹)	PdBI/30m
O ¹³ CS	18→17	218199	1.07 (0.40)	0.63 (0.04)	~60 %
H ₂ CO	3 _{0,3} →2 _{0,2}	218222	41.11 (1.13)	4.51 (0.19)	~10%
HC ₃ N	24→23	218325	2.40 (0.38)	1.84 (0.34)	~100%
CH ₃ OH	4 _{2,0} →3 _{1,0}	218440	12.54 (0.49)	2.80 (0.03)	~20%
H ₂ CO	3 _{2,2} →2 _{2,1}	218476	10.80 (0.42)	3.26 (0.56)	~30%
H ₂ CO	3 _{2,1} →2 _{2,0}	218760	10.54 (0.42)	2.98 (0.11)	~30%
OCS	18→17	218903	3.11 (0.44)	3.29 (0.05)	~100%
C ¹⁸ O	2→1	219560	32.85 (0.20)	2.47 (0.10)	<10%
HNCO	10 _{3,8} →3 _{7,*}	219657	< 1.13	1.04 (0.11)	~100%
	10 _{3,7} →3 _{6,*}				
HNCO	10 _{2,9} →9 _{2,8,*}	219734	1.91 (0.53)	2.13 (0.12)	~100%
	10 _{2,8} →9 _{2,7,*}	219737			
HNCO	10 _{0,10} →9 _{0,9}	219798	3.14 (0.42)	2.12 (0.12)	~70%
H ₂ ¹³ CO	3 _{1,2} →2 _{1,1}	219909	1.96 (0.37)	1.18 (0.11)	~60%
SO	5 ₆ →4 ₅	219949	43.20 (2.75)	8.65 (0.21)	~20%
E-CH ₃ OH	8 ₀ →7 ₁	220078	3.59 (0.95)	3.95 (0.14)	~100%
¹³ CO	2→1	220399	144.49 (1.67)	5.54 (0.13)	<1%
CH ₃ CN	12 ₅ →11 ₅	220641	2.18 (0.64)	2.50 (0.13)	~100%
CH ₃ CN	12 ₄ →11 ₄	220679	2.00 (0.25)	2.20 (0.08)	~100%
CH ₃ CN	12 ₃ →11 ₃	220709	1.68 (0.65)	2.16 (0.70)	~100%
CH ₃ CN	12 ₂ →11 ₂	220730	2.07 (0.58)	2.05 (0.46)	~100%
CH ₃ CN	12 ₀ →11 _{0,*}	220747	5.14 (0.71)	4.05 (0.52)	~100%
	12 ₁ →11 _{1,*}	220743			~100%

¹Comparison between the flux measured with the 30m and PdBI telescopes for all the lines detected with the 30m single-dish telescope.

²Velocity-integrated flux density in the 30m spectrum.

³Velocity-integrated flux density towards the emission peak.

*Blended lines.

plies opacities of ~ 10 in the main isotopologue line. Since the line opacities are very high, the rotational diagram analysis is not valid and the resulting rotation temperature in the ground state is severely over-estimated. Instead, we derived the CH₃CN column density assuming $T_{\text{rot}}=405$ K (the same as in the $\nu_8=1$ vibrational level) and an opacity of ~ 10 for the CH₃CN 12₄→11₄ line and obtained $N(\text{E-CH}_3\text{CN})=N(\text{A-CH}_3\text{CN})=2.6\times 10^{18}$ cm⁻², i.e., a total (A+E) CH₃CN column density of 5.2×10^{18} cm⁻². With these parameters, we fit the high energy rotational lines with a source size of $\approx 0.07''$ (125 AU). The uncertainty in the source size comes from the assumed rotation temperature. By varying the rotation temperature between 250 and 600 K we would obtain sizes of 100–160 AU. Note that these sizes are quite small, similar to typical scales of circumstellar disks.

This compact source model successfully predicted the intensities of the high excitation lines, but the intensities of the low energy transitions were severely underestimated. The only way to fit the whole spectrum was to consider a two-component model: (i) the compact one described above, and (ii) a more extended second component that is filling the beam. We fit the $K<4$ lines with $N(\text{E-CH}_3\text{CN})=N(\text{A-CH}_3\text{CN})=2.5\times 10^{14}$ cm⁻² and $T_{\text{rot}}=350$ K for this extended component. We tried with a temperature of 250 K obtained from the fitting of the $E_{\text{rot}}<400$ K $\nu_8=1$ lines, but this lower temperature would overestimate the $K=0$ and $K=1$ lines. Besides the assumed value is within the uncertainty of this fit ($=250^{+110}_{-59}$ K).

Our estimate of the total methyl cyanide column density relies on the ¹³C isotopologue line. Of course there is also the possibility that the CH₃¹³CN 12₄→11₄ line is contaminated by another line and its real intensity is lower. We did not find any good candidate at this frequency. One line of EA-(CH₃)₂CO is very close in frequency but the emission of this line is very weak

(see also Sect. 4.8). Furthermore, the small sizes derived for other species (see following sections) prompted us to consider the two-component model as the most likely one. We would also like to point out that we refer to a beam filling component at the spatial resolution of our observations (~ 1900 AU) as “extended component”. This component would not encompass the entire envelope.

We also looked for the deuterated compounds in our spectrum. The most abundant species CH₂DCN and CHD₂CN have no intense lines in the observed frequency range. Only CD₃CN has three intense transitions at 219.965, 219.983 and 219.993 GHz. We have detected the three lines but need a very low rotation temperature, $T_{\text{rot}}=40$ K, to fit them. Because of this surprisingly low rotation temperature, we consider that a misidentification is possible and keep the derived column density as an upper value to the real one. Several weak lines of CH₃NC were identified, a molecule so far only detected towards Sgr B2 (Cernicharo et al. 1988). Unfortunately, most of them are blended or partially blended. Assuming that CH₃NC is coming from the CH₃CN compact core, we calculated a CH₃NC column density of 1.5×10^{16} cm⁻², i.e., about 350 times lower than that of CH₃CN. Since we have only one unblended line, we keep this detection as tentative.

4.2. Isocyanic acid: HNCO, HN¹³CO

The HNCO lines are well fitted with $T_{\text{rot}}=260^{+4}_{-5}$ K and $N(\text{HNCO})=1.6\times 10^{15}$ cm⁻² (see Fig. 2 and Table 2). In our frequency range, most of the lines of HN¹³CO are blended with those of the main isotopologue, therefore we cannot estimate the line opacities. Comparing with the 30m spectrum, we calculated that the interferometer is missing about 20% of the flux of the

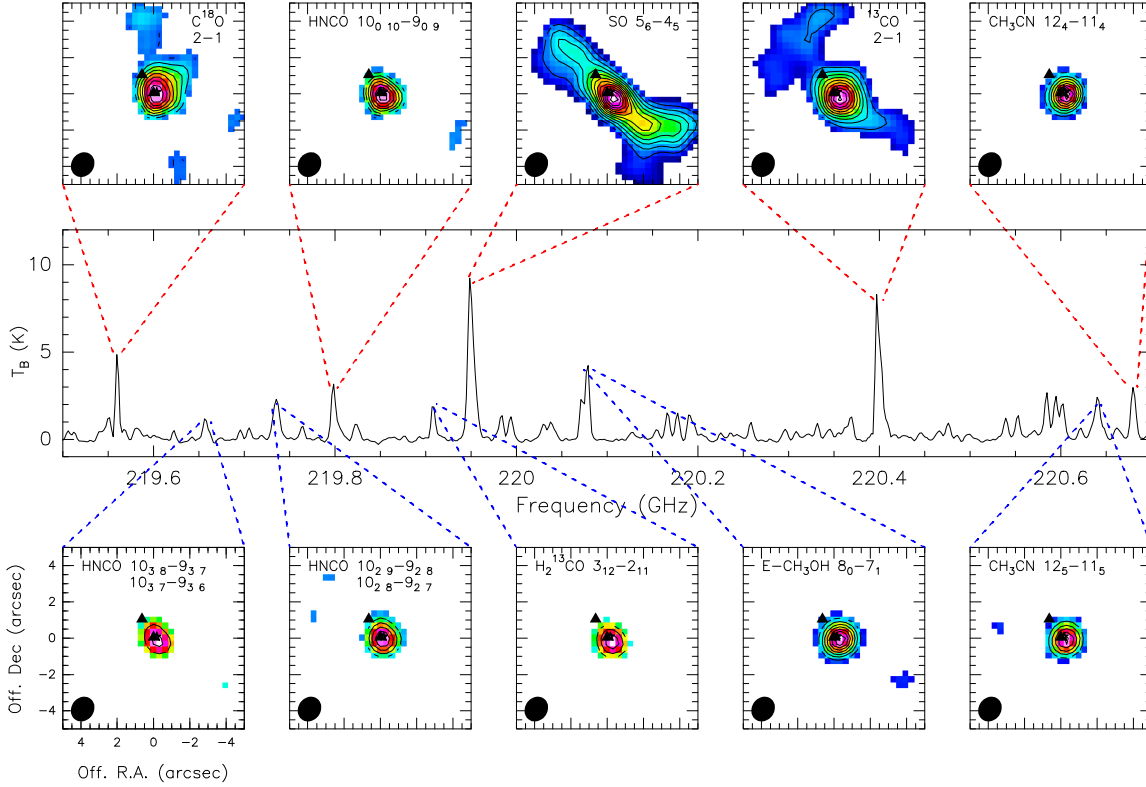


Fig. 1. *Middle:* PdBI spectrum towards the emission peak. *Top and bottom:* Integrated intensity maps of the most intense lines in the portion of spectrum between 219.5 GHz and 220.7 GHz. In all the panels the contours start and increase at steps of $3 \times \sigma$. Sigma and peak values in $\text{Jy}/\text{beam} \times \text{km s}^{-1}$ are: 0.10, 2.47 (C^{18}O 2-1); 0.12, 2.12 (HNC 10_0-9_0); 0.21, 8.65 (SO 5_6-4_5); 0.22, 7.28 (^{13}CO 2-1); 0.08, 2.20 (CH_3CN 12_4-11_4); 0.11, 1.04 (HNC 10_3-9_3); 0.12, 2.13 (HNC 10_2-9_2); 0.11, 1.18 (H_2 ^{13}CO $3_{1,2}-2_{1,1}$); 0.14, 3.95 ($\text{E-CH}_3\text{OH}$ 8_0-7_1); 0.13, 2.5 (CH_3CN 12_5-11_5). Filled triangles indicate the water masers as observed with the NRAO Very Large Array (Aina Palau, private communication). The masers trace the direction of the youngest outflow (Fuente et al. 2001) that is also clearly seen in the SO and ^{13}CO images. The (0,0) position is the phase center of the interferometric observations: $21^{\text{h}}43^{\text{m}}01^{\text{s}}.7$, $+66^{\circ}03'23''.6$ (J2000).

low energy lines, showing that there is an extended component. For this reason, we adopt the beam filling solution. We looked for the isomer HCNO and the deuterated compound DNCO but unfortunately they do not have intense transitions in the sampled frequency range.

4.3. Methyl formate: $A\text{-CH}_3\text{OCHO}$, $E\text{-CH}_3\text{OCHO}$

We detected more than sixty lines of $A\text{-CH}_3\text{OCHO}$ and $E\text{-CH}_3\text{OCHO}$ in our spectrum, both in the $\nu_7=0,1$ vibrational states, the latter at $E_{\text{vib}}=188.40$ K. We tried to fit a rotational diagram to each vibrational state separately in order to measure the rotation and vibrational temperatures independently but this was not possible. The dynamical range of the E_u 's within each vibrational level is very small and the uncertainties in the integrated intensities are too large to obtain a good fit. However we could get a reasonable fit by considering the two vibrational levels together (see Table 2). We measured $T_{\text{vib,rot}} \sim 265_{-69}^{+139}$ K, slightly lower than that of CH_3CN but still in good agreement taking into account the associated uncertainties. We fixed the temperature and varied the source size to fit the lines. The best fit was obtained with a size of $\sim 0.1''$. Even with this small size, the opacities of

the CH_3OCHO $\nu=0$ lines are always ≤ 1.3 suggesting that our estimate of the rotation temperature is reliable. Unfortunately, the lines of the ^{13}C isotopologues are blended with other species and it was not possible to have an estimate of their column densities. We used a weak feature at 128.952 GHz to derive an upper limit to the total column density of $^{13}\text{CH}_3\text{OCHO}$ of $< 3.0 \times 10^{17} \text{ cm}^{-2}$ in the $\sim 0.1''$ core, which would imply an upper limit to the total (A - + E -) column density of $< 2.0 \times 10^{19} \text{ cm}^{-2}$ assuming $^{12}\text{C}/^{13}\text{C}=65$. This allows us to say that the methyl formate column density is accurate within a factor of 4. About deuteration, we have three detected lines at 219242 MHz, 218730 MHz and 219132 MHz that would correspond to CH_3OCDO and CH_2DOCHO . The first two lines are blended with lines of $\text{EE-}(\text{CH}_3)_2\text{CO}$ which makes the derived deuterium fraction more uncertain. Taking into account the contribution of acetone, we fitted the intensities of the three lines assuming a deuterium fraction of ~ 0.06 .

4.4. Ethyl cyanide: $\text{CH}_3\text{CH}_2\text{CN}$

The detection of eight lines of $\text{CH}_3\text{CH}_2\text{CN}$ strongly confirms the identification of this species. Although three of them are

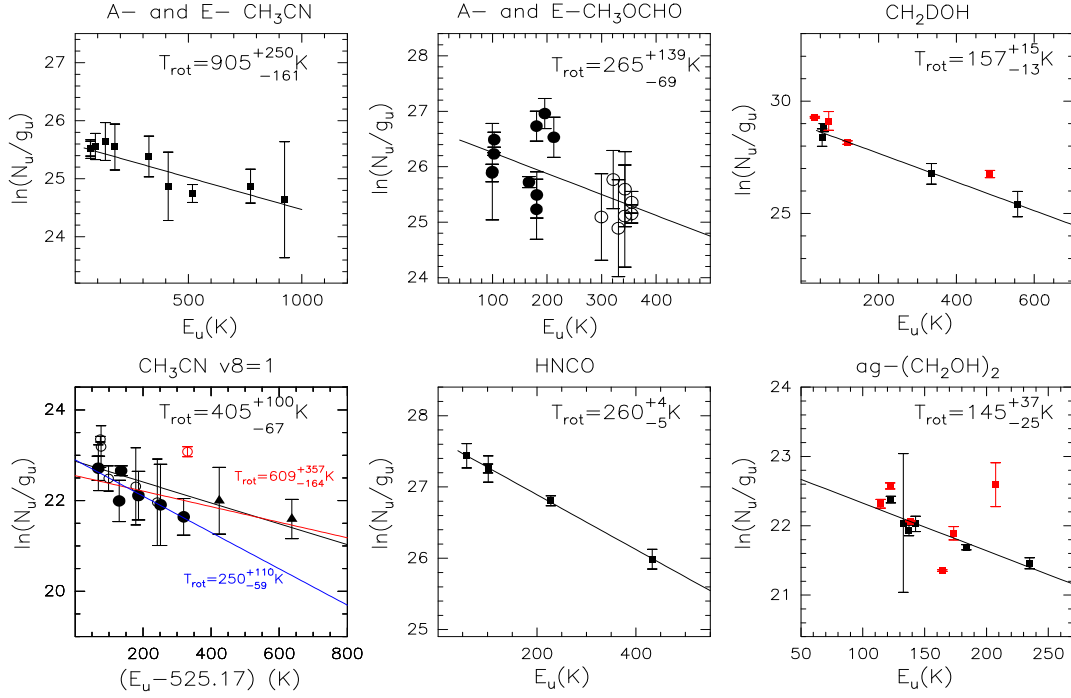


Fig. 2. Results of the rotational diagrams for $\text{CH}_3\text{CN } \nu=0$, $\text{CH}_3\text{CN } \nu_8=1$, CH_3OCHO , HNC , CH_2DOH and $\text{ag}'\text{-(CH}_2\text{OH)}_2$. The high rotation temperature fitted to the $\text{CH}_3\text{CN } \nu=0$ rotational diagram is the consequence of the lines being optically thick and is not considered in our modeling (see Sect. 4.1). In the rotational diagram of the $\text{CH}_3\text{CN } \nu_8=1$ vibrational state we use different symbols for: blended lines (empty circles), isolated or partially blended lines (filled circles) and the points with $E_{\text{rot}} > 400$ K (triangles). The three straight lines correspond to the least square fittings with: all the points (black), only unblended lines (red), unblended lines with $E_{\text{rot}} < 400$ K (blue). For CH_3OCHO , the points corresponding to the $\nu=0$ lines are indicated with filled squares and those of $\nu_1=1$ with empty circles. The parameters of the transitions used in the rotation diagrams are listed in Tables A.3-8. Red points have not been used in the least square fitting because they correspond to heavily blended lines.

heavily blended, the other five lines are enough to identify this species. The lines belong to the ground state and to the lowest energy vibrational states at $E_{\text{vib}}=297.12$ K (Daly et al. 2013). We tried to fit the rotational diagram but unfortunately the points did not follow a clear pattern and we could not determine the rotation temperature. Hence, we fixed the rotation temperature to a value of 200 K (a reasonable value from the rotational temperatures measured with the other species, see Table 2) and fitted the column density. A beam averaged column density value of $5.2 \times 10^{14} \text{ cm}^{-2}$ was derived from the intensity of the most intense lines. The fit improved assuming that the emission comes from a compact source with a diameter of $\sim 0.1''$, because some lines become optically thick. This is the solution we finally adopted (see Table 3). We searched for the lines of the ^{13}C isotopologues and the deuterated species but the lines were too weak to obtain a significant upper limit to their column densities.

4.5. Methanol: A- and E- CH_3OH , A- and E- $^{13}\text{CH}_3\text{OH}$, CH_2DOH

Only five lines of methanol (including the A- and E- species and their vibrational states) were detected and their intensities were not consistent with LTE. This is not unexpected since the emission of the low energy lines is optically thick and extended (see Table 1). We searched for the lines of $^{13}\text{CH}_3\text{OH}$ and the deuterated species CH_2DOH . Ten lines of CH_2DOH were detected. We removed from our fit the lines that could be blended with

other more intense lines and we still kept 4 “clean” lines that allowed us to derive the results shown in Fig. 2 and Table 2. The rotation temperature of CH_2DOH , $\sim 157^{+15}_{-13}$ K, is lower than that of CH_3CN suggesting that it arises from a different region within the hot core. Based on the different spatial distribution of the high excitation and low excitation lines of methanol, FU05 proposed the existence of two components: a hot component towards the hot core and a colder component that extends along the outflow direction. Although the two components are expected to contribute to the total CH_2DOH emission, its low rotation temperature suggests that it is dominated by the extended one.

For $^{13}\text{CH}_3\text{OH}$, we detected two lines of the $\nu_1=0$ vibrational state (220323 and 221282 MHz) and one (221424 MHz) of the $\nu_1=1$ state. Although the emissions of the low energy lines of the main isotopologue are extended (see Table 1), we considered that the emissions of the ^{13}C -methanol lines come mainly from the compact source. The line at 220323 MHz is heavily blended and cannot be used to estimate the ^{13}C -methanol column density. Using the other two lines we fitted a vibrational/rotation temperature of ~ 238 K and a total $^{13}\text{CH}_3\text{OH } \nu_1 = 0, 1$ column density of $5.3 \times 10^{18} \text{ cm}^{-2}$. In order to estimate the uncertainty in our estimate of the ^{13}C -methanol column density, we repeated the fit by fixing the rotation temperature to 200 K and 400 K. The derived column densities are $3.0 \times 10^{18} \text{ cm}^{-2}$ and $6.1 \times 10^{18} \text{ cm}^{-2}$, respectively, which suggests that our estimate of the ^{13}C -methanol column density is accurate within a factor of 2.

Since the CH_3OH lines are optically thick, we derived the methanol column density from $^{13}\text{CH}_3\text{OH}$ assuming that all the

Table 3. NGC 7129 FIRS 2 hot core model

Species	$T_{\text{rot}}(\text{K})$	$N_X (\text{cm}^{-2})^1$	$D('')^2$	
CH ₃ CN $\nu=0$	405	5.2×10^{18}	0.07	E ⁴
	350	5.0×10^{14}	BF ³	G ⁵
CH ₃ CN $\nu_8=1$	405	7.0×10^{16}	0.07	G
CH ₃ ¹³ CN $\nu=0$	405	8.0×10^{16}	0.07	E
	350	7.7×10^{12}	BF	G
CH ₃ NC*	405	3.0×10^{16}	0.07	G
CD ₃ CN*	40	$<5.0 \times 10^{13}$	BF	G
CH ₃ OH $\nu_1=0,1$	238	3.4×10^{20}	0.12	G
	157 ⁶	2.0×10^{166}	BF	G
¹³ CH ₃ OH $\nu=0$	238	4.2×10^{18}	0.12	G
¹³ CH ₃ OH $\nu_1=1$	238	1.1×10^{18}	0.12	G
CH ₂ DOH	157	1.4×10^{16}	BF	G
CH ₃ OCHO $\nu=0$	265	3.4×10^{18}	0.12	E
CH ₃ OCHO $\nu_1=1$	265	1.7×10^{18}	0.12	E
CH ₃ OCDO	265	1.6×10^{17}	0.12	G
S-CH ₂ DOCHO	265	8.0×10^{16}	0.12	G
A-CH ₂ DOCHO	265	8.0×10^{16}	0.12	G
CH ₃ CH ₂ CN	200	9.4×10^{16}	0.12	E
CH ₃ CH ₂ CN $\nu_{13}=1 / \nu_{21}=1$	200	2.9×10^{16}	0.12	E
CH ₂ CHCN $\nu_{11}=0,1$	200	$<9.4 \times 10^{17}$	0.12,	G
CH ₃ CH ₂ OH	200	3.0×10^{18}	0.12	E
CH ₃ COCH ₃	200	1.0×10^{15}	BF	G
(o+p)-H ₂ CO	200	7.0×10^{17}	0.34	E
(o+p)-H ₂ ¹³ CO	200	1.1×10^{16}	0.34	E
(o+p)-D ₂ CO	200	5.9×10^{15}	0.34	E
OCS	200	2.0×10^{18}	0.32	E
OCS $\nu_2=1$	200	2.4×10^{16}	0.32	E
O ¹³ CS	200	3.1×10^{16}	0.32	E
HC ₃ N	200	2.0×10^{16}	0.20	E
HC ₃ N $\nu_7=1$	200	2.0×10^{15}	0.20	E
DC ₃ N*	200	3.1×10^{14}	0.20	G
SO	200	$>>2.4 \times 10^{15}$	BF	E
S ¹⁸ O	200	$<8.0 \times 10^{15}$	0.6	G
SO ₂	200	6.0×10^{15}	BF	G
³⁴ SO ₂	200	2.7×10^{14}	BF	G
HNCO	260	1.6×10^{15}	BF	E
HN ¹³ CO	260	2.5×10^{13}	BF	E
(o+p)-H ₂ ¹³ CS	200	1.2×10^{15}	0.60	E
(o+p)-HDCS*	200	1.0×10^{15}	0.60	E
HCOOH	100	9.5×10^{18}	0.12	E
H ¹³ COOH	100	1.5×10^{17}	0.12	E
HCOOD*	100	1.0×10^{17}	0.12	E
CH ₃ OCH ₃	200	4.0×10^{18}	0.12	E
CH ₃ CHO $\nu_1=0$	100	4.0×10^{15}	BF	G
CH ₃ CHO $\nu_1=1$	100	5.6×10^{14}	BF	G
CH ₃ CHO $\nu_1=2$	100	1.1×10^{14}	BF	G
aGg ⁻ -(CH ₂ OH) ₂	145	2.0×10^{15}	BF	G
(o+p)-H ₂ CCO*	200	6.7×10^{14}	BF	G
CH ₂ OHCHO	265	1.0×10^{15}	BF	G
NH ₂ CHO*	200	3.0×10^{14}	BF	G

¹Estimated column densities. ²Diameter of the emission region for the compact component assuming a disk morphology. ³BF: Beam filling component. ⁴E: The disk diameter estimated from our modeling. ⁵G: only a guess because the size of the disk cannot be constrained on basis of our data. ⁶The fit to this component is not reliable because the lines suffers from spatial filtering and opacity effects (see text). *Tentative detection

¹³CH₃OH emission comes from the compact component and ¹²C/¹³C=65. Then we added an extended component to fit the rest of lines. The value obtained for the CH₃OH column density in the extended component is not reliable because the intensities of the main isotopologue lines are affected by spatial filtering and opacity effects. Moreover, the separation of the methanol emission in these two components is model-dependent since we

fixed the size of the compact core in our calculations. The beam average CH₃OH column density derived from ¹³CH₃OH is, however, reliable as long as the ¹³C-isotopologue is optically thin regardless of the detailed spatial distribution of methanol within the observational beam. For this reason, we used this value to calculate the deuterium fraction, [CH₂DOH]/[CH₃OH]=0.02. This is an average value within the hot core.

4.6. Trans- and Gauche- ethanol: T- and G-CH₃CH₂OH

We detected six ethanol lines which includes four from T-CH₃CH₂OH and two from the G conformer that is at 60 K above the T-state. However, only three lines are clearly detected (at 218554, 218655, and 220155 MHz) since the other are significantly blended with transitions from other species or U-lines. Because of this, we could not apply the rotational diagram technique. Instead, we assumed a rotation temperature of $T_{\text{rot}}=200$ K, and derived the column densities using the most intense lines. We assumed a size of $\sim 0.1''$ to better fit the data published by FU05 (see Sect.5). The results are shown in Table 3.

4.7. Acetone: AA-(CH₃)₂CO, AE-(CH₃)₂CO, EA-(CH₃)₂CO, EE-(CH₃)₂CO

Several lines of acetone were detected in our spectrum (218773, 219076, 219220, 219242, 219264, 220355, 220466, 220764, 220962 MHz) being the most intense at 219220, 219242 and 219264 MHz. Because many of them are blended, it is not possible to determine an accurate rotation temperature. We assumed $T_{\text{rot}}=200$ K and obtained a total (AA+EA+AE+EE) beam average column density of $1.0 \times 10^{15} \text{ cm}^{-2}$.

4.8. Formaldehyde: H₂CO

Three lines of p-H₂CO and one of o-H₂¹³CO were detected in the PdBI spectrum. The lines of the main isotopologue are optically thick and most of their emission has been filtered by the interferometer (see Table 1). Because of the large fraction (85%) of missing flux in the main isotopologue line, we are surely missing an extended component. According with Fig. 1, the emission of the o-H₂¹³CO is unresolved by our observations. Besides, FU05 derived a size of $0.58 \pm 0.24'' \times 0.40 \pm 0.24''$ for the D₂CO emission. Based on these results, we were able to fit all the lines of this work and FU05 with an (ortho+para)-H₂¹³CO column density of $1.1 \times 10^{16} \text{ cm}^{-2}$ and (ortho+para)-D₂CO column density of $5.9 \times 10^{15} \text{ cm}^{-2}$, and a source with a diameter of $0.34''$ ($\sim 426 \text{ AU}$). We assume $T_{\text{rot}}=200\text{K}$ and an ortho-to-para ratio of 3.

There are no H₂C¹⁸O and HDCO lines in the frequency range of our observations that we could use to further constrain our model.

4.9. Carbonyl sulfide: OCS, O¹³CS

The $J=19 \rightarrow 18$ rotational lines of the ground vibrational states of OCS and O¹³CS lie in the range of wavelengths covered by our observations. We measured $T_b[\text{OCS } 19 \rightarrow 18]/T_b[\text{O}^{13}\text{CS } 19 \rightarrow 18] \sim 5$. Comparing the 30m and PdBI spectra, we discarded the possibility that this low intensity ratio is a consequence of the spatial filtering. The opacity of the OCS $19 \rightarrow 18$ line must be very high, $\tau \sim 12$. Assuming $T_{\text{rot}}=200$ K, we derived a OCS column density of $\sim 2 \times 10^{18} \text{ cm}^{-2}$ and a source size of $\sim 0.32''$ (400 AU), four times that derived for the compact component

of CH₃CN. In our spectrum, we also detected two lines of the OCS $\nu_2=1$ vibrational state at $E_{\text{vib}}=748.8$ K (see Table A.1). Assuming the same source size, the intensities of these lines imply a vibrational temperature, $T_{\text{vib}}=170$ K, in agreement with the rotational temperature we assumed. The same assumptions are used to fit the OC³³S J=19→18 line in FU05.

4.10. Sulfur monoxide: SO, S¹⁸O

Only the intense line of SO at 219949 MHz was detected. From its intensity and assuming $T_{\text{rot}}=200$ K, we derived a beam averaged SO column density of 2.4×10^{15} cm⁻². The emission of this line is extended (see Table 1 and Fig. 1) and, most likely, optically thick. There are no lines of ³⁴SO, ³³SO and/or S¹⁸O in the spectrum that could be used to determine the line opacity. As commented in Sect. 5 a possible detection of S¹⁸O in the spectrum published by FU05 suggests that the column density could be as much as a factor of ~600 higher (see Sect.5 and Table 3). Unfortunately this line is blended with other intense lines which makes the estimate uncertain. We consider our fitted value as a lower limit to the real one.

4.11. Sulfur dioxide: SO₂, ³⁴SO₂

One SO₂ line at 219276 MHz and two ³⁴SO₂ lines at 219355 and 221115 MHz, respectively were detected. These lines are reasonably fitted using $T_{\text{rot}}=200$ K, a beam averaged SO₂ column density of 6×10^{15} cm⁻² and $^{32}\text{S}/^{34}\text{S}=22$. The SO₂ line is optically thin providing a good estimate of the total number of SO₂ molecules within our beam. On the other hand, we could not estimate an accurate value of the opacity that would allow us to constrain the size of the emitting region. We checked that the SO₂ line would be optically thin even if all the emission arises from the 0.1'' compact core, however.

4.12. Cyanoacetylene: HCCCN, HCCCN $\nu_7=1$, DCCCN, HCCNC

We detected one HC₃N line at 218325 MHz and two lines of the vibrational state $\nu_7=1$ at 218861 MHz and 219174 MHz, respectively, although the one at 219174 MHz is blended with an intense ethanol line. In addition, we tentatively detected the H¹³CCCN 25→24 line. Unfortunately the frequency of the H¹³CCCN line is close to that of the ¹³CO 2→1 line and could have some contribution from its wing. Assuming that the isotopologue line is not blended with ¹³CO, we fit this line with $T_{\text{rot}}=200$ K and $N(\text{H}^{13}\text{CCCN})=8.8 \times 10^{14}$ cm⁻² and a source size of ~0.20'' which implies an upper limit to the HC₃N column density of $<5.7 \times 10^{16}$ cm⁻². This value, however, overestimates the intensity of the lines of the main isotopologue, that are better fitted with $N(\text{HCCCN})=2.0 \times 10^{16}$ cm⁻². We adopt the latter solution and conclude that our column density is accurate within a factor of 3. There is a weak feature at 219490 MHz that could correspond to DCCCN J=26→25. Since this line is very weak and there is no other DCCCN line in the spectrum that could confirm the detection, we will consider it as a tentative detection and use its intensity to derive an upper limit to the DCCCN column density of $N(\text{DCCCN})/N(\text{HCCCN}) < 0.016$. We could have detected one line of HCCNC at 218558 MHz but it is blended with an intense ethanol line. Therefore we can only derive a lower limit to the $N(\text{HCCCN})/N(\text{HCCNC})$ column density ratio of >13 .

4.13. Acetaldehyde: CH₃CHO

Very few intense lines of CH₃CHO are found in the observed wavelength range and some of them are blended with others from abundant species. We detected without blending: the 220446 MHz line of E-CH₃CHO, and marginally the 221222 MHz line of A-CH₃CHO $\nu_7=1$, the 219780 MHz line of A-CH₃CHO $\nu_7=2$, and 221216 MHz line of E-CH₃CHO $\nu_7=2$. All these lines were fitted assuming $T_{\text{vib}}=100$ K. Making the additional assumption that $T_{\text{rot}}=T_{\text{vib}}$, we derived a total beam averaged A+E CH₃CHO column density of 4×10^{15} cm⁻² in the $\nu=0$ ground state. In this case, the lines of the ¹³C isotopologue were not detected. Like for other oxygenated molecules, we assumed that the source is extended relative to our beam. Although the firm detections in the 218-221 GHz frequency range are only a few, this model is fully confirmed by the good match to the data published by FU05 (see Sect. 5).

4.14. Formic acid: HCOOH

Two lines of HCOOH, one at 218938 MHz and the other at 220038 MHz were detected in our spectrum. However their line intensities were not consistent with thermalized optically thin emission. Since the two lines have very similar E_u , this discrepancy cannot be due to a wrong rotation temperature. Spatial filtering cannot be the cause of this discrepancy, because such an intense line should have been detected in the 30m spectrum. However the Einstein spontaneous emission coefficient, A_{ij} , of the 220038 MHz line is 10 times lower than that of the 218938 MHz line which results in a higher opacity of the former for the same physical conditions. We propose that the high opacity of the line at 220038 MHz causes the anomalous line intensity ratio. The detection of H¹³COOH at 219341.849 MHz also argues in favor of a high column density of HCOOH in this source. We can reasonably fit both lines of HCOOH and that of H¹³COOH assuming $T_{\text{rot}}=100$ K, a total HCOOH column density of 9.5×10^{18} cm⁻² and a source size of ~0.1''. The profile of the H¹³COOH line is wider than expected (see Fig. A.2), suggesting some contribution from the outflow or partial blending with other line. Because of this possible blending, the integrated intensity of this line is uncertain by a factor of 2. We selected the solution that best fitted the 218938 MHz line. The fit to the HCOOH line at 220038 MHz is not perfect but this is not worrying because our model is not adequate to reproduce the profile of very optically thick lines. In fact the intensity of this line is not sensitive to the HCOOH column density in the range of column densities we are dealing with. Some HCOOH lines were also observed by FU05. As seen in Fig. 5, the lines are reasonably reproduced with our values. We have searched for the DCOOH and HCOOD lines in our spectrum and found one transition of HCOOD at 218541 MHz from which we derive $N(\text{HCOOD})/N(\text{HCOOH}) \approx 0.01$ as long as both species are coming from the same region. Since we have only one line of HCOOD and it is at 4σ , we indicated this detection as tentative in Table 3.

4.15. Dimethyl ether: CH₃OCH₃

We detected four unblended lines of CH₃OCH₃, at 218492, 219301, 220847, and 220893 MHz. The other lines of this species are blended with intense lines. Assuming that the source is filling the beam, we derived $T_{\text{rot}}=500$ K and $N(\text{CH}_3\text{OCH}_3)=2 \times 10^{16}$ cm⁻². We considered that this apparently high rotation temperature was an opacity effect and obtained a

better fit assuming $T_{\text{rot}}=200$ K, $N(\text{CH}_3\text{OCH}_3)=4\times 10^{18}$ cm^{-2} and a source diameter of $0.1''$. These parameters are consistent with the non-detection of the ^{13}C isotopologues and we adopted them.

4.16. Ethylene glycol: $a\text{Gg}'-(\text{CH}_2\text{OH})_2$, $g\text{Gg}'-(\text{CH}_2\text{OH})_2$

The $a\text{Gg}'$ conformer of ethylene glycol, together with methyl formate, is one of those with the highest number of lines in our spectrum. We detected twelve lines, and seven were unblended. We used these seven unblended lines to derive a rotation temperature of 145 K and a beam averaged column density of $N(a\text{Gg}'-(\text{CH}_2\text{OH})_2)=2.3\times 10^{15}$ cm^{-2} (see Fig. 2 and Table 2). One of the lines, that at 218576 MHz was removed from the final fit since it was very far from the intensity traced by the other lines (see Fig. 2) and is certainly blended with something else. In this case, we did not have information about the transitions of the ^{13}C -isotopologues and deuterated species. The emission is compatible with the beam filling assumption although we cannot discard a smaller size.

We also searched for $g\text{Gg}'-(\text{CH}_2\text{OH})_2$ in our spectrum. We have a good match with 8 lines that can be assigned to this species (218712, 219097, 219389, 219410, 220763, 220448, 220887, 221596 MHz). Modeling the spectrum, we obtain that 5 additional lines are also present in our data but blended with other species. However there are 2 lines, at 218144 MHz and 220249 MHz, that should have been detected and do not appear in the spectrum. These lines have similar energies as the previous ones and their absence cannot be explained with a simple excitation argument. This species has not been detected in any other source thus far. Waiting for confirmation, we do not include it in the model.

4.17. Ketene: H_2CCO

We detected one *o*- H_2CCO line at 220177 MHz and one *p*- H_2CCO at 221545 MHz with similar intensity. The first transition is at $E_u=62.4$ K and the second one $E_u=894.8$ K. It is not possible to fit both lines assuming reasonable physical conditions and optically thin emission. One possibility is that the line at 221545 MHz is not ketene. In this case, we can fit the other line assuming a rotation temperature of $T_{\text{rot}}=200$ K and a beam averaged ortho+para H_2CCO column density of 6.7×10^{14} cm^{-2} , where we have assumed an ortho-to-para ratio of 3. Another possibility is that the emission is optically thick in both lines. In this case, we need a ketene column density of 4.0×10^{18} cm^{-2} in a compact $\sim 0.1''$ region. There is no line of the ^{13}C isotopologue in the observed frequency range that would allow us to determine the opacities. The deuterated compounds have no intense transitions in the observed wavelength range either. We selected the optically thin case adopting a conservative approach. Taking into account the uncertainty in its column density, we do not use this species in our comparison with other sources.

4.18. Glycolaldehyde: CH_2OHCHO , Formamide: NH_2CHO

There are thirteen intense lines of glycolaldehyde in the sampled wavelength range. From these, six are not blended with other features and do not have any other likely identification. Assuming $T_{\text{rot}}=200$ K, we estimated a beam averaged column density of 1.0×10^{15} cm^{-2} . Only one line of NH_2CHO lies in our spectrum. It is at 218459 MHz and is blended with a line of T-ethanol. Our fit to T-ethanol failed to predict the high intensity of the observed feature suggesting some contribution from

NH_2CHO . The total intensity would be consistent with a beam averaged formamide column density of 3.0×10^{14} cm^{-2} .

4.19. Vinyl cyanide: CH_2CHCN

We detected two rotational lines, at 218675 MHz and 220345 MHz, that could correspond to CH_2CHCN . The intense line at 220345 MHz is overlapped with one of CH_3CN . Some features of the $\nu_{11}=1$ vibrational state at an energy of 328.4 K could have also been detected but are blended with other more intense lines. Since we could not determine the rotation temperature, we assumed the fixed value of $T_{\text{rot}}=200$ K and the same source size as the chemically related species CH_3CN , i.e., a diameter of $\sim 0.1''$. But our fit was very bad. The intensities of the lines at 220345 MHz and 218675 MHz cannot be accounted by LTE models. We were not able to obtain a better fit by varying the rotation temperature and/or the source size. One possibility is that the intensity of one of the lines is wrong because of baseline uncertainties or spatial filtering. The second possibility is that our identification is false. Since we do not have a better candidate for the 220345 MHz line, we derived an upper limit to the vinyl cyanide column density using its line intensity and fixing the rotation temperature to 200 K. This compound is quite abundant in massive hot cores (see (López et al. 2014), and this upper limit is interesting for comparison with this kind of objects.

5. The hot core model

Based on the calculations explained in Sect. 4, we propose the hot core model shown in Table 3. This model is not unique and some parameters, especially source sizes, are quite uncertain. However it cannot be done better. Higher spatial resolution are required to better constrained the spatial structure. Fortunately, the total number of molecules in our beam is well constrained, especially when we have detected the ^{13}C isotopologue or the emission is optically thin, which is the case for most species. Our model is self-consistent, i.e., once a molecule is included, its isotopologues and deuterated compounds are also included. For isotopologues, we assume $^{12}\text{C}/^{13}\text{C}=65$, $^{16}\text{O}/^{18}\text{O}=650$, $^{32}\text{S}/^{34}\text{S}=22$ and $^{34}\text{S}/^{33}\text{S}=6$ (Chin et al. 1995, Milam et al. 2005). The column densities of the deuterated species are calculated independently to determine the deuterium fractions. When possible we directly compare the deuterated compound with the ^{13}C isotopologue, that is expected to have similar fractional abundance, in order to avoid opacity effects in the derived column density ratio. The obtained values of deuterium fractions are: ~ 0.06 for methyl formate, ~ 0.02 for methanol, ~ 0.008 for the doubly deuterated formaldehyde, ~ 0.01 for DC_3N , and <0.01 for HCOOD (see Table 3). Of course these are average values in the hot core since the hydrogenated and deuterated species could have different spatial distributions. Using MADEX, we have synthesized the total spectrum assuming LTE, the parameters shown in Table 3 and convolving with a circular beam of $\sim 1.4''$. The obtained spectrum is compared with observations in Figs. A.1-4. Our fit is reasonably good taking into account the simplicity of our model. There are, however, two frequency ranges 218.0-219.12 GHz and 221.46-221.62 where the agreement is poor. One reason is possible observational errors. Note that the second region is at the end of the observed frequency range where the passband calibration is more uncertain. But the existence of intense "U" lines suggests the existence of a population of COMs that have not been identified yet.

An important test for our model is to reproduce the interferometric observations published by FU05 with a higher an-

Table 4. Comparison of rotation temperatures between hot cores and hot corinos

Hot core/corino	L_{\odot}	$T_{\text{rot}}(\text{CH}_3\text{CN})$	$T_{\text{rot}}(\text{X})$	ref.
IRAS 16293-2422	6.9–23	~150-390 K	~60 K (CH_3CHO)	Cazaux et al. (2003), Bisschop et al. (2008) Pineda et al. (2012)
IC 1396 N	<300	~100 K		Neri et al. (2007), Fuente et al. (2009)
IRAS 22198+6336	370	~100 K	~120 K ($\text{CH}_3\text{CH}_2\text{OH}$)	Sánchez-Monge et al. (2010), Palau et al. (2011)
NGC 7129 FIRS 2	480	~400 K	~120 K ($\text{aGg}'\text{-(CH}_2\text{OH)}_2$)	This work
AFGL 5142	2300		~140–210 K ($\text{CH}_3\text{CH}_2\text{OH}$)	Palau et al. (2011)
Orion KL	~ 10^4	400–600 K	~100-200 K ($\text{CH}_3\text{OCH}_3, \text{OCS}$)	Tercero et al. (2010), Beuther et al. (2011), Brouillet et al. (2013), Bell et al. (2013)

gular resolution of $0.63'' \times 0.46''$. We synthesized the spectrum assuming the same parameters as in Table 3 but convolving with a smaller beam, $\sim 0.52''$, and compared with FU05 observations (see Fig. A.5). We find a remarkably good agreement for most of the species which confirmed that our model was not far from reality.

We identified the line at 231143 MHz in FU05 as H_2^{13}CS providing an estimate of the H_2CS abundance in the hot core (see Table 3). However we have only one line of the ^{13}C isotopologue and the identification could be wrong. A similar situation occurs for S^{18}O . We have detected one line at 228272 MHz but it is blended with intense CH_3OCHO and CH_3OCOD features. From this line we estimate a S^{18}O column density of $8 \times 10^{15} \text{ cm}^{-2}$ within the $\sim 0.52''$ ($\sim 650 \text{ AU}$) beam. Because of the blending, this estimate is model-dependent and suffers from larger uncertainty.

An important discrepancy between our model and FU05 observations comes from G+ethanol. There are two predicted G+ethanol lines, 228491 MHz and 228560 MHz that do not appear in the FU05 spectrum while all the T-ethanol lines are correctly reproduced. One possibility is that we have a lower kinetic temperature than assumed since the G+ethanol is 60 K higher in energy than T-ethanol. But the temperature would have to be unreasonably low, $< 50 \text{ K}$, to reproduce the observations. These lines are close to the edge of the spectral band and could suffer from some instrumental effects.

In Table A.2 we give a list with our new identifications of the data published by FU05. In this work we have identified more lines and found some misidentifications. The lines previously identified as c- C_3D are instead carried by CH_3CHO . In fact, CH_3CHO is the carrier of most of the lines in the band centered at 231.3 GHz. We have a handful of lines around the ^{13}CS frequency without any plausible identification. One possibility is that we are observing high velocity gas emitting in the ^{13}CS 5 \rightarrow 4 line, but this would imply an outflow with velocities as high as 50 km s^{-1} . We have not seen such high velocities in the CO single-dish and interferometric spectra (Fuente et al. 2001, FU05). Therefore, we think that there are still some unidentified lines at these frequencies. The intense lines at 228307 MHz, 228363 MHz, 228427 MHz and 228467 MHz, although identified, are poorly reproduced by our model. We have not found any simple way to improve the agreement between our model and observations. Either these lines are far from the LTE approximation or we are still missing important species. Additional observations could help to discern their origin.

The observations presented in this paper have significantly contributed to the understanding of the spectra published by FU05 proving that observations in a large range of frequencies are needed for the correct line identification.

Table 5. Average fractional abundances¹

	$T_{\text{dust}}=50 \text{ K}$	$T_{\text{dust}}=400 \text{ K}$
$M_{\text{gas+dust}} (M_{\odot})$	1.8	0.46
$N_{\text{H}_2} (\text{cm}^{-2})$	2.0×10^{24}	5.0×10^{23}
$\text{CH}_3\text{CN} (^{13}\text{C})^2$	6×10^{-9}	3×10^{-8}
CH_3OCHO	2×10^{-8}	7×10^{-8}
$\text{CH}_3\text{CH}_2\text{CN}$	4×10^{-10}	2×10^{-9}
CH_2CHCN	$< 3 \times 10^{-9}$	$< 2 \times 10^{-8}$
$\text{CH}_3\text{OH} (^{13}\text{C})$	1×10^{-6}	5×10^{-6}
CH_2DOH	7×10^{-9}	3×10^{-8}
$\text{CH}_3\text{CH}_2\text{OH}$	1×10^{-8}	4×10^{-8}
CH_3COCH_3	5×10^{-10}	2×10^{-9}
$\text{H}_2\text{CO} (^{13}\text{C})$	2×10^{-8}	8×10^{-8}
D_2CO	2×10^{-10}	7×10^{-10}
$\text{OCS} (^{13}\text{C})$	5×10^{-8}	2×10^{-7}
HC_3N	2×10^{-10}	8×10^{-10}
SO_2	3×10^{-9}	1×10^{-8}
HNCO	8×10^{-10}	3×10^{-9}
$\text{H}_2\text{CS} (^{13}\text{C})$	7×10^{-9}	3×10^{-8}
$\text{HCOOH} (^{13}\text{C})$	3×10^{-8}	1×10^{-7}
CH_3OCH_3	1×10^{-8}	6×10^{-8}
CH_3CHO	2×10^{-9}	1×10^{-8}
$\text{aGg}'\text{-(CH}_2\text{OH)}_2$	1×10^{-9}	4×10^{-9}
CH_2OHCHO	5×10^{-10}	2×10^{-9}

¹ Average fractional abundance in a disk with a diameter of $\sim 1.4''$.

² Derived from the ^{13}C isotopologue assuming $^{12}\text{C}/^{13}\text{C}=65$.

6. Discussion

6.1. Physical conditions

It is known that hot cores are heterogenous objects where different species are coming from different regions with different physical conditions (see. e.g. Beuther et al. 2011, Brouillet et al. 2013, Bell et al. 2013). For this reason, we only compare rotation temperatures measured with the same molecular species.

Methyl cyanide is easily thermalized for the densities prevailing in hot cores and hence a good thermometer of the molecular gas. The rotational diagram shows that the temperature in the FIRS 2 hot core is $\approx 400 \text{ K}$. This temperature is similar to that measured in massive hot cores. Beuther et al. (2011) proposed the existence of a warm component of $600 \pm 200 \text{ K}$ in the Orion hot core based on submillimeter CH_3CN lines as observed with the Submillimeter Array (SMA). More recently, Bell et al. (2013) estimated a rotation temperature of $\sim 220 \text{ K}$ towards IRc2 and $\sim 400 \text{ K}$ in the hot spot located $\sim 14''$ NE using data from the 30m telescope. Lower temperatures, however, are found in hot corinos. Bisschop et al. (2008) derived an upper limit of $< 390 \text{ K}$ in IRAS 16293-2422 A and B based on interferometric SMA data. Fuente et al. (2009) derived a rotation temperature of $97 \pm 25 \text{ K}$ in the hot core located in the IM protocluster IC 1396 N. A similar rotation temperature, $\sim 100 \text{ K}$, was de-

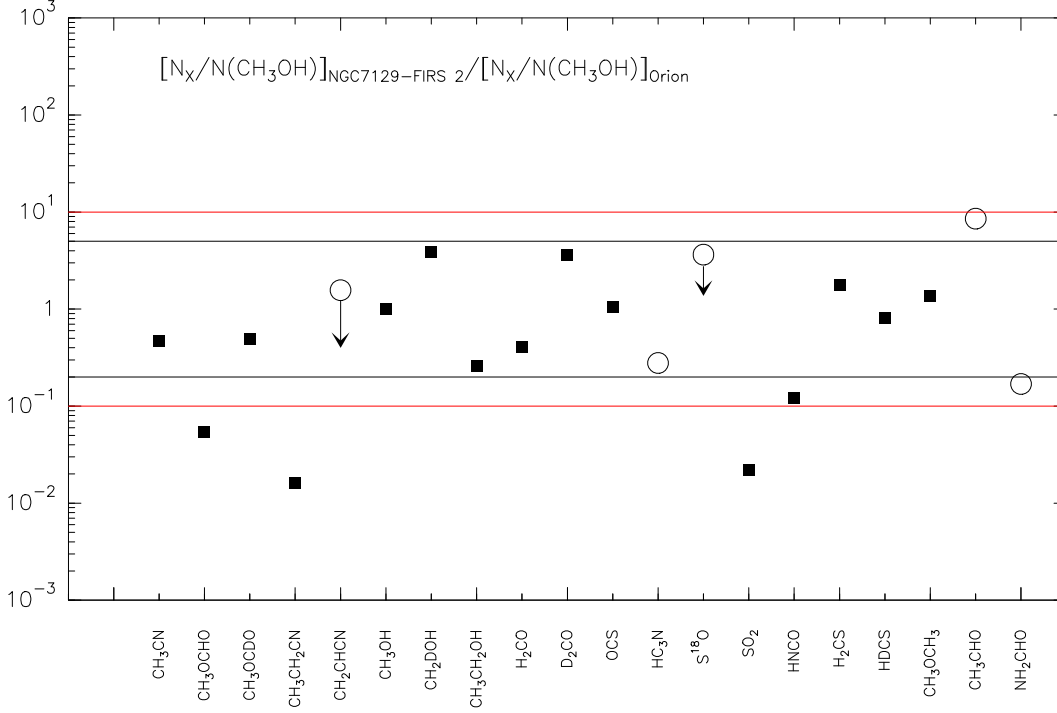


Fig. 3. Comparison of the molecular abundances in FIRS 2 and the Orion hot core (see Table 6). All the molecular abundances have been normalized to that of CH_3OH . Black horizontal lines indicate the loci of the FIRS 2 values that differ by less than a factor of 5 from those of Orion. Red lines indicate the same but for a factor of 10. Empty circles indicate doubtful values.

Table 6. Comparison between FIRS 2 and Orion KL

	FIRS 2 ¹ N (cm ⁻²)	Orion KL ² N (cm ⁻²)	Refs ³
CH_3CN	1.3×10^{16} (¹³ C) ⁴	1.2×10^{16} (¹³ C)	Bell et al. (2014)
CH_3OCHO	3.7×10^{16}	2.9×10^{17} (¹³ C)	Carvajal et al. (2009), Haykal et al. (2014)
CH_3OCDO	1.1×10^{15}	1.0×10^{15}	Margulès et al. (2010)
$\text{CH}_3\text{CH}_2\text{CN}$	8.8×10^{14}	2.3×10^{16} (¹³ C)	Daly et al. (2013)
CH_2CHCN	$< 6.9 \times 10^{15}$	2.4×10^{15}	López et al. (2014)
CH_3OH	2.5×10^{18} (¹³ C)	1.1×10^{18} (¹³ C)	Kolesníková et al. (2014)
CH_2DOH	1.4×10^{16}	1.5×10^{15}	Neill et al., (2013)
$\text{CH}_3\text{CH}_2\text{OH}$	2.2×10^{16}	3.6×10^{16}	Kolesníková et al. (2014)
H_2CO	4.1×10^{16} (¹³ C)	4.3×10^{16} (¹³ C)	Neill et al. (2013)
D_2CO	3.4×10^{14}	4.2×10^{13}	Turner, B.E. (1990)
OCS	1.0×10^{17} (¹³ C)	4.2×10^{16} (¹³ C)	Tercero et al. (2010)
HC_3N	4.1×10^{14}	7.7×10^{15} (¹³ C)	Esplugues et al. (2013b)
S^{18}O	$< 1.5 \times 10^{15}$	2.2×10^{14}	Esplugues et al. (2013a)
SO_2	6.0×10^{15}	1.1×10^{17}	Esplugues et al. (2013a)
HNCO	1.6×10^{15}	5.5×10^{15} (¹³ C)	Marcelino et al. (2009)
H_2CS	1.4×10^{16} (¹³ C)	3.3×10^{15} (¹³ C)	Tercero et al. (2010)
HDCS	1.8×10^{14}	9.5×10^{13}	Tercero et al. (2010)
HCOOH	6.9×10^{16} (¹³ C)	4.9×10^{13}	Turner, B.E. (1991)
CH_3OCH_3	2.9×10^{16}	9.0×10^{15}	Comito et al. (2005)
CH_3CHO	5.0×10^{15}	2.8×10^{14}	Turner, B. E. (1991)
NH_2CHO^*	3.0×10^{14}	9.6×10^{14}	Motiyenko et al. (2012)

¹ Average molecular column densities in a disk with a diameter of $1.4''$. It is calculated with the expression $N = N_c \times (D''/1.4'')^2 + N_{ex}$ where N_c and D are the column density and size (diameter) of the compact component, respectively, and N_{ex} , the column density of the beam filling component as shown in Table 3.

² Average molecular column densities considering a region of $15''$ of diameter towards Orion KL. We assume a beam filling factor of 0.44 for the hot core component (size= $10''$).

³ References for the Orion column densities.

⁴ Derived from the ¹³C isotopologues assuming ¹²C/¹³C=65 for FIRS 2 and ¹²C/¹³C=50 for Orion.

rived by Sánchez-Monge et al. (2010) in the hot core associated with IRAS 22198+6336. Although the luminosity of FIRS 2 is similar, our observations suggest the existence of a warmer gas component (~ 400 K) in FIRS 2 than in IC 1396 N and IRAS 22198+6336. IC 1396 N is a protocluster with three young stellar objects (YSOs). Although the total luminosity is similar to that of FIRS 2, the luminosity of each YSO is lower and probably closer to that of an Ae star, i.e., $< 100 L_{\odot}$. IRAS 22198+6336 is morphologically similar to FIRS 2. Sánchez-Monge et al. (2010) detected only the K-lines with $E_u=100-300$ K, while we used lines with $E_u>600$ K in this study. It is possible that a warmer component remains hindered in IRAS 22198+6336 and would require higher sensitivity observations of transitions with higher E_u to be detected. In fact, FU05 determined a gas temperature of 50–100 K in FIRS 2 from lower sensitivity observations of the $\text{CH}_3\text{CN } 5_K \rightarrow 4_K$ ladder, from lines with $E_u=13-154$ K.

The rotational diagrams of the oxygenated species give lower rotation temperatures than with CH_3CN . We derived rotation temperatures between 100 K and 200 K from the CH_2DOH , CH_3CHO and $\text{aGg}'-(\text{CH}_3\text{OH})_2$ lines and between 200 K and 300 K from CH_3OCHO and HNCO . Palau et al. (2011) derived rotation temperatures of $\sim 100-150$ K in the IM hot cores in IRAS 22198+6336 and AFGL 5142 from the ethanol lines. Rotation temperatures of around 100 K are also derived in Orion from CH_3OCH_3 , methyl formate, deuterated methanol and OCS (Tercero et al. 2010, Peng et al. 2012, Brouillet et al. 2013). Therefore, we do not detect significant differences between the rotation temperatures measured with these O-bearing species between IM and massive hot cores. Lower rotation temperatures, ~ 50 K, are measured with CH_3OCHO in IRAS 16293-2422 (Pineda et al. 2012).

In Table 4, we show a summary of the rotation temperatures derived from different molecules and for different hot cores. The comparison is not totally fair since CH_3CN and the O-bearing molecules could come from different regions. This is the case of IRAS 16293-2422, where CH_3CN is coming mainly from the southern component (A) and the O-bearing molecules from the northern one (B) (Bisschop et al. 2008). As commented above, different regions are associated with O- and N-bearing molecules in Orion. Towards the other hot cores, the spatial resolution provided by the existing observations is lower, preventing us from resolving regions with different chemistries. Nevertheless, it seems that there is a weak trend with the maximum gas temperature increasing from low to massive hot cores as measured with CH_3CN . There is no trend for the O-bearing molecules.

This suggests a scenario in which the O-bearing molecules are more abundant in extended regions with temperatures ~ 100 K in both hot cores and corinos. Instead, CH_3CN probes the hottest region of the core, and its rotation temperature increases with the luminosity. Of course, there is a problem with the spatial scales that are different for low-mass and massive stars. But, taking into account that massive stars are more distant, this would favor the interpretation of higher temperatures in the latter. Therefore, within the limitations of our analysis, we can conclude that there is a trend of increasing temperature from hot corinos to massive hot cores. It is not so clear between IM and massive stars. As we discuss, there is no obvious difference between FIRS 2 and Orion.

Another important parameter is the total amount of gas in the hot core. One possibility is to calculate it from the dust continuum emission assuming a dust temperature and a dust emissivity value. FU05 adopted a dust temperature of $T_{\text{dust}}=100$ K and $\kappa_{\nu}=0.015 (1300/\lambda (\mu\text{m})) \text{ cm}^2 \text{ g}^{-1}$ and derived a total gas+dust mass of $2 M_{\odot}$ in the hot core FIRS 2. More recently, Palau et

al. (2013) derived a similar value ($1.8 M_{\odot}$) assuming $T_{\text{dust}}=50$ K and $\kappa_{1.3\text{mm}}=0.00899 \text{ cm}^2 \text{ g}^{-1}$. Our results suggest that at least a fraction of the dust must be at $T_{\text{dust}}=400$ K. Assuming $T_{\text{dust}}=400$ K and $\kappa_{1.3\text{mm}}=0.01 \text{ cm}^2 \text{ g}^{-1}$, we obtain a lower limit to the gas+dust mass of $0.46 M_{\odot}$. Therefore, the total gas+dust mass of the FIRS 2 hot core is uncertain in a factor of ~ 4 . In Table 5 we show the average molecular abundances in a region of $1.4''$ assuming $M=1.8 M_{\odot}$ and $0.46 M_{\odot}$ for the hot core mass, respectively. When detected, we used the ^{13}C isotopologue to determine the total average molecular column density which is more reliable. As discussed in Sect. 4, the uncertainties in the molecular column densities would add an error of a factor $\leq 4-5$ to these values.

6.2. Comparison with the Orion hot core

The hot core associated with FIRS 2 is extraordinarily rich in complex molecules. We have detected glycolaldehyde and tentatively formamide that had been detected only in a few objects thus far. Glycolaldehyde was detected in Sgr B2 (Hollis et al. 2000, Halfen et al. 2006, Requena-Torres et al. 2008), the massive hot core G31.41+0.31 (Beltrán et al. 2009) and more recently towards the hot corino IRAS 16293-2422B (Jorgensen et al. 2012, Zapata et al. 2013). Formamide has been detected in Orion (Motiyenko et al. 2012), Sgr B2 (Belloche et al. 2013), a handful of massive prototypical hot cores (Adande et al. 2013) and IRAS 16293-2422 (Kahane et al. 2013). In Figs. A.1-4, we compare the FIRS 2 spectrum with that of the Orion hot core as observed with the 30m telescope (Tercero et al. 2010). Surprisingly, there is a good match between both spectra, both in number of lines and relative line intensities, suggesting that both hot cores have similar chemical characteristics. Of course, this is a qualitative comparison and we need to put it on quantitative grounds to establish firm conclusions.

In Table 6 and Fig. 3 we compare the molecular column densities in FIRS 2 and Orion KL. For this comparison, in FIRS 2, we have used the average column densities in a region of $1.4''$. The reason is that the sizes of the emitting regions are not determined for most of the species (see Table 3). One needs to know the rotation temperature and the line opacities independently, to be able to determine the source size. In many cases we do not have detected the ^{13}C isotopologue that would allow us to derive the line opacities. In others, the number of unblended lines is not enough to determine the rotation temperature and we had to assume a reasonable value. On the contrary, the number of molecules per beam is a quite well determined parameter as long as the emission is optically thin which is a reasonable assumption for many complex species. When detected, we used the ^{13}C isotopologue to determine the total average column density.

Towards Orion KL, the molecular emission is formed of 4 physically different components: hot core, plateau, compact ridge and extended ridge. The plateau has a chemistry characteristic of a shocked region and is considered to be associated with the shocks produced by a past eruptive episode. The extended ridge is the parent cloud that hosts the cluster of young stars. The compact ridge is a small ($\sim 15''$) ‘‘U’’ shaped feature that is characterized for being very rich in complex O-bearing molecules. The hot core is a very compact source ($6''-10''$) particularly rich in complex N-bearing molecules. We cannot resolve different regions within the FIRS 2 hot core, therefore we consider that the FIRS 2 hot core is comparable to the hot core (HC) and the compact ridge (CR) Orion components together. In Table 6 we show the average column densities of the HC+CR Orion components in a region of $15''$. To estimate this value,

we have summed up the column densities of the HC and CR weighted by their respective filling factors: 0.44 for HC (assuming a size of $10''$) and 1 for the CR. When possible, we used the ^{13}C isotopologues to determine the Orion column densities (see Table 6). We assume $^{12}\text{C}/^{13}\text{C}=50$ for Orion (Comito et al. 2005, Tercero et al. 2010). Some authors, like Neill et al. (2013) and Comito et al. (2005) used a size of $10''$ for the CR. We have multiplied their column densities by 0.44 to account for the different adopted source sizes. For CH_3CHO we have adopted the value of Turner (1991). This author did not distinguish among the different Orion components (hot core, plateau, compact ridge and extended ridge) and we have taken the total value. For this reason this point is drawn as an empty circle in Fig. 3. In the case of D_2CO , Turner (1990) assumed a source size of $15''\times 25''$ that is consistent with ours.

In Fig. 3 we compare the column densities of FIRS 2 and Orion normalized to methanol. Normalization is required if one wants to compare the relative abundances of the different species in the warm gas. Methanol is commonly used to make this kind of normalization in hot cores (Öberg et al. 2011). Instead we could have used methyl cyanide for the normalization but we would have obtained essentially the same trend. As it is clearly seen in Table 6, it would simply produce an increase in all the ratios by factor of 2.

Most of the relative molecular abundances in FIRS 2 agree with those in Orion within a factor of 5, which is quite good taking into account the uncertainty due to the unknown spatial structure of the molecular emission and opacity effects. Only a few molecules have abundances significantly different in both hot cores: CH_3OCHO , $\text{CH}_3\text{CH}_2\text{CN}$, HNCO and SO_2 have fractional abundances more than 10 times lower in FIRS 2 than in Orion. In the case of CH_3OCHO , we have not detected the ^{13}C isotopologues in FIRS 2 and our column density could be slightly underestimated. As discussed in Sect. 4.3, our estimate is accurate within a factor of 4. Increasing the methyl formate by a factor of 4 would push the methyl formate back to the region within the two black lines in Fig. 3, although still in the lower end. In the case of HNCO , the lines of the main isotologue are blended with those of the ^{13}C isotopologue preventing us from a direct estimate of the line opacities. Looking at the top of the Figure, there is a group of molecules that are more abundant in FIRS 2 by more than a factor of 4–5. These molecules are: CH_2DOH , D_2CO and CH_3CHO . As commented above, the value of CH_3CHO in Orion is uncertain. However the differences observed in CH_2DOH and D_2CO could be significant. In the following Section, we discuss possible scenarios to explain these differences.

6.3. Sequential formation of complex molecules in hot cores/corinos

Although gas phase reactions can play a role, surface chemistry dominates the formation of COMs. The large sensitivity of surface chemistry on physical parameters, especially the dust temperature, can also explain the observed chemical differentiation within a hot core and among different hot cores. For example, Caselli et al. (1993) found that complex N-bearing species are more easily formed if the dust temperature (T_{dust}) is about 40 K during the collapse phase. This is primarily due to the higher mobility of carbon and the shortage of hydrogen (H , H_2) on the grain surfaces. A similar argument has been used by Öberg et al. (2011) to explain the over-abundance of $\text{CH}_2/3$ -rich molecules in hot cores and corinos compared with molecular outflows. Öberg

et al. (2011) studied a number of cores associated with outflows, low-mass cores observed with single-dish telescopes (tracing envelopes at ~ 5000 AU spatial scales), low-mass cores observed with interferometers (tracing warmer material at ~ 500 AU), and an average of high-mass hot molecular cores from Bisschop et al. (2007), and they found that HCO-rich molecules are in general more abundant than $\text{CH}_3/2$ -rich molecules in outflows and envelopes of low-mass YSOs, while the situation is reversed for low-mass inner envelopes/disks and high-mass YSOs. They proposed a sequential formation of complex molecules, starting with HCO-rich molecules as long as CO ice is abundant, followed by $\text{CH}_3/2$ -rich molecules at higher ice temperatures.

In Fig. 4 we present an updated version of the figure by Öberg et al. (2011) complemented with abundances of three intermediate-mass hot cores observed with interferometers (at ~ 500 AU scales, from this work and Palau et al. 2011), and the new Orion data. In the Figure, symbols in warm colors (orange, red) correspond to $\text{CH}_3/2$ -rich molecules, while symbols in cold colors (blue/black) correspond to HCO-rich molecules. Our new results for the intermediate-mass hot core FIRS 2 are in line with previous measurements towards IM hot cores at disk-scales (~ 500 AU). Putting all these data together, we do not find a clear trend for the abundances of the $\text{CH}_3/2$ -rich and HCO-rich molecules with the stellar mass. Considering only interferometric observations, the CH_3CHO abundance seems to decrease with the stellar mass. However, the abundance of methyl formate, the only other HCO-rich molecule considered, is larger in Orion than in IM hot cores and hot corinos. Orion is the only source in which we have been able to use the ^{13}C isotopologue to derive the methyl formate abundance. If the methyl formate lines were typically optically thick in hot cores/corinos, this would have produced an underestimate of the CH_3OCHO abundance in the rest of objects. Using the upper limit to the emission of the ^{13}C isotopologue, we have estimated that the methyl formate abundance in FIRS 2 is accurate within a factor of 4. Even considering an uncertainty of a factor of 4 in the CH_3OCHO abundances towards low mass and IM YSOs, the $[\text{CH}_3\text{OCHO}]/[\text{CH}_3\text{OH}]$ ratio would be larger in Orion than in these objects. Besides, the $[\text{CH}_3\text{OCHO}]/[\text{CH}_3\text{OH}]$ ratio seems to increase from the low-mass to the IM sample. We can only compare two HCO-rich molecules in Fig. 4. Therefore we cannot know if methyl formate is a special case (see also Taquet et al. 2012). Further observations in IM and massive hot cores are required to have a deeper insight into the chemistry of this molecule and other HCO-rich species.

We have yet to discuss the deuterium fractions in FIRS 2 and Orion. Deuterated species whose deuteration requires surface chemistry, such as D_2CO , present higher abundances in the warm regions associated with low-mass protostars. Loinard et al. (2003) searched for the doubly deuterated form of formaldehyde (D_2CO) in a large sample of young stellar objects. D_2CO was detected in all low-mass protostars, with $[\text{D}_2\text{CO}]/[\text{H}_2\text{CO}]$ ratios of 2–40%. On the other hand, no detection was obtained towards massive protostars (where $[\text{D}_2\text{CO}]/[\text{H}_2\text{CO}] < 0.5\%$). This is consistent with the value reported by Turner (1990) in Orion. If the hot cores associated with massive stars are older and/or significantly denser than those surrounding low-mass objects, gas phase chemistry could have had the time to reset the deuterium fractions to values close to the cosmic D/H ratio. The longer time of the evaporated molecules in gas phase in would also affect the abundances of the COMs that can be formed in warm gas-phase chemistry (e.g. CH_2CHCN).

An alternative explanation could be that the temperature of the envelope material accreting onto the high mass protostars is

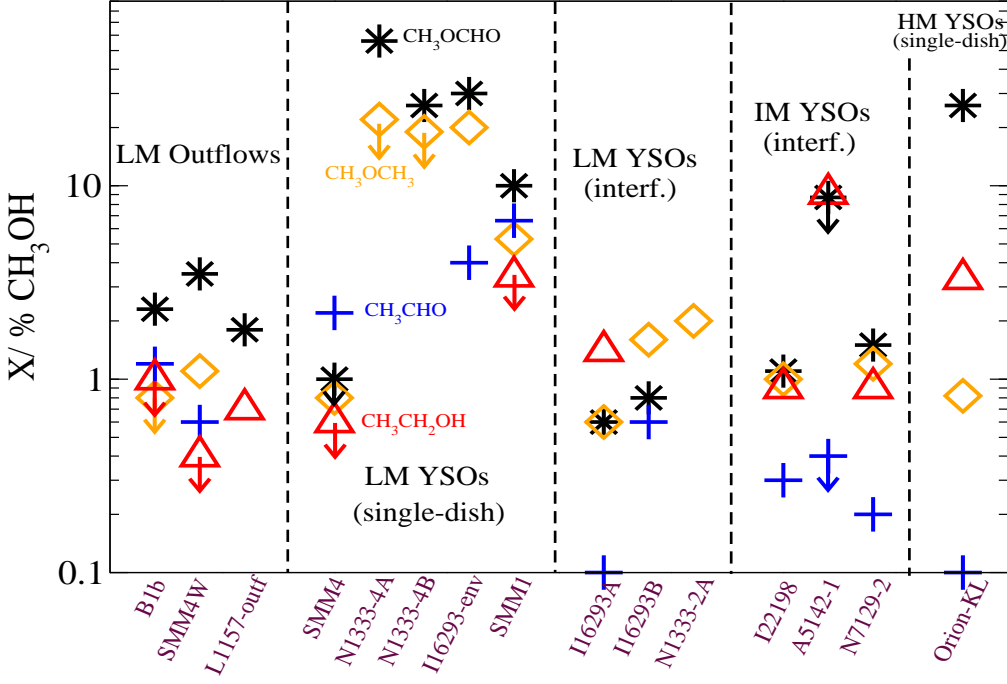


Fig. 4. Abundance of complex organic molecules relative to CH_3OH for different types of sources, after Öberg et al. (2011): from left to right, low-mass outflows, low-mass YSOs observed with single-dish (tracing envelopes), low-mass YSOs observed with interferometers (tracing the inner envelope/disk at ~ 500 AU spatial scale), intermediate-mass YSOs observed with interferometers (also at 500 AU spatial scale, this work and Palau et al. 2011), and Orion (references in Table 6). Symbols with cold colors correspond to HCO-rich molecules (black: CH_3OCHO ; blue: CH_3CHO), and symbols with warm colors correspond to $\text{CH}_3/2$ -rich molecules (orange: CH_3OCH_3 ; red: $\text{CH}_3\text{CH}_2\text{OH}$).

larger than 30 K (Fontani et al. 2002). In this case the deuterium fractionation efficiency in the gas phase is strongly reduced before the hot core phase as the standard H_2D^+ route ($\text{H}_3^+ + \text{HD} \rightarrow \text{H}_2\text{D}^+ + \text{H}_2$) also starts to proceed from left to right. Moreover, at $T_{\text{dust}} > 30$ K there is no way that deuteration can be enhanced on the grain surfaces. The reason is that H and D are easily evaporated before reacting on the surface (see e.g. Cazaux et al. 2011). The higher temperature during the collapse would also affect the formation of COMs in grain mantles. As CO does not efficiently freezes-out at these values of T_{dust} , the formation of HCO-rich molecules would be strongly diminished too. As commented above, methyl formate could be an exception of this rule.

6.4. Carbon budget

We have used the column densities shown in Table 3 to estimate the Carbon gas phase budget in the FIRS 2 hot core. Apart from CO and its isotopologues, most of the Carbon is locked in methanol with a total column density of $\sim 3.4 \times 10^{20} \text{ cm}^{-2}$ in the compact component of the hot core. Taking into account the rest of molecules, the Carbon column density reaches to $\sim 4 \times 10^{20} \text{ cm}^{-2}$ in this small region. One problem to derive absolute abundances is that we do not know the total column density of gas in the inner $R < 0.05''$ region. Based on higher angular resolution observations, FU05 derived a size of $0.72'' \times 0.52''$ for the continuum source that account for 75% of the continuum emission and a point source that contributes with 25% of

the flux. Adopting this value for the fraction of continuum flux coming from the compact component of the hot core and a total gas mass of $0.46 M_{\odot}$ (see Section 6.1), the total column density of molecular hydrogen would be $2 \times 10^{25} \text{ cm}^{-2}$ and the fractional abundance of the Carbon locked in COMs relative to H nuclei, $\sim 1.0 \times 10^{-5}$. This value is 36 times lower than the solar value of the Carbon abundance ($\text{C}/\text{H} \sim 3.6 \times 10^{-4}$, Anders & Grevesse 1989) and suggests that methanol and COMs (at least those considered in this paper) are not the main reservoirs of Carbon in hot cores.

It is also useful to compare methanol with C^{18}O . Again we have the problem of the unknown spatial distribution of the C^{18}O emission within our interferometric beam. We can derive a lower limit to the C^{18}O abundance assuming that the emission is optically thin and fills the beam. Adopting $T_{\text{rot}} = 400$ K, we derive $N(\text{C}^{18}\text{O}) = 1.5 \times 10^{17} \text{ cm}^{-2}$ and $N(\text{CO}) = 9.4 \times 10^{19} \text{ cm}^{-2}$. This solution, however, is not compatible with the non-detection of the C^{18}O 9 \rightarrow 8 line by Fuente et al. (2012) and we cannot reconcile the PdBI and Herschel results by lowering the temperature down to $T_{\text{rot}} = 200$ K. The optically thick solution seems more reasonable. Assuming again that the gas temperature is 400 K and that the C^{18}O emission is optically thick ($T_B \approx T_{\text{rot}}$), we derive an effective diameter of $0.15''$ for the C^{18}O emitting region. In this case, our results are compatible with the Herschel upper limit to the C^{18}O 9 \rightarrow 8 line and the column density of CO would be $> 10^{22} \text{ cm}^{-2}$ in the compact component of the hot core.

7. Conclusions

FIRS 2 is probably the youngest IM protostar studied thus far and, as such, an excellent template upon which to base interpretations of other IM and massive star forming regions. The interferometric observations presented in this paper proved that this IM protostar hosts a hot core extraordinarily rich in complex molecules. The gas kinetic temperature as measured with methyl cyanide, is around 400 K, similar to that of the Orion hot core and higher than typical rotation temperatures in hot corinos. A detailed comparison of the chemistry of FIRS 2 with Orion shows that the fractional abundances of most molecules relative to that of CH₃OH agree within a factor of 5, that is reasonable taking into account the uncertainties of our column density estimates. Only CH₃CH₂CN, HNC, SO₂, CH₂DOH, D₂CO and CH₃CHO present a significant disagreement, with CH₃CH₂CN, HNC and SO₂ being more abundant in Orion, and CH₂DOH, D₂CO and CH₃CHO, in FIRS 2. Since the physical conditions are similar in both hot cores, only different initial conditions (warmer pre-collapse and collapse phase in the case of Orion) and/or different crossing time of the gas in the hot core can explain this behavior. FIRS 2 is a YSO in which most of the accreting envelope still maintains an overall temperature lower than 30 K, allowing deuteration to proceed unhindered, while complex N-bearing molecules like CH₃CH₂CN are not efficiently formed, unlike the Orion hot core.

Acknowledgements. We thank the Spanish MINECO for funding support from grants CSD2009-00038, AYA2009-07304, and AYA2012-32032. DJ is supported by the National Research Council of Canada and by a Natural Sciences and Engineering Research Council of Canada (NSERC) Discovery Grant. A.P. is supported by the Spanish MICINN grant AYA2011-30228-C03-02 (co-funded with FEDER funds), and by the AGAUR grant 2009SGR1172 (Catalonia).

References

- Adande, G. R., Woolf, N. J., & Ziurys, L. M. 2013, *Astrobiology*, 13, 439
- Alonso-Albi, T., Fuente, A., Crimier, N., et al. 2010, *A&A*, 518, A52
- Anders, E., & Grevesse, N. 1989, *Geochim. Cosmochim. Acta*, 53, 197
- Bell, T. A., Cernicharo, J., Viti, S. et al. 2013, *A&A* accepted
- Belloche, A., Müller, H. S. P., Menten, K. M., Schilke, P., & Comito, C. 2013, *A&A*, 559, A47
- Beltrán, M. T., Codella, C., Viti, S., Neri, R., & Cesaroni, R. 2009, *ApJ*, 690, L93
- Beuther, H., Zhang, Q., Greenhill, L. J., et al. 2005, *ApJ*, 632, 355
- Beuther, H., Zhang, Q., Reid, M. J., et al. 2006, *ApJ*, 636, 323
- Bisschop, S. E., Jørgensen, J. K., Bourke, T. L., Bottinelli, S., & van Dishoeck, E. F. 2008, *A&A*, 488, 959
- Blake, G. A., Sutton, E. C., Masson, C. R., & Phillips, T. G. 1987, *ApJ*, 315, 621
- Bottinelli, S., Ceccarelli, C., Lefloch, B., et al. 2004b, *ApJ*, 615, 354
- Bottinelli, S., Ceccarelli, C., Neri, R., et al. 2004a, *ApJ*, 617, L69
- Bottinelli, S., Ceccarelli, C., Williams, J. P., & Lefloch, B. 2007, *A&A*, 463, 601
- Brouillet, N., Despois, D., Baudry, A., et al. 2013, *A&A*, 550, A46
- Carvajal, M., Margulès, L., Tercero, B., et al. 2009, *A&A*, 500, 1109
- Cazaux, S., Tielens, A. G. G. M., Ceccarelli, C., et al. 2003, *ApJ*, 593, L51
- Cazaux, S., Caselli, P., & Spaans, M. 2011, *ApJ*, 741, L34
- Cernicharo, J., Kahane, C., Guélin, M., & Gómez-González, J. 1988, *A&A*, 189, L1
- Cernicharo, J. 2012, in *Proceedings of the European Conference on Laboratory Astrophysics*, Eur. Astron. Soc. Publ. Ser, eds. C. Stehlé, C. Joblin, & L. d'Hendecourt
- Cernicharo, J., Tercero, B., Fuente, A., et al. 2013, *ApJ*, 771, L10
- Chin, Y.-N., Henkel, C., Whiteoak, J. B., Langer, N., & Churchwell, E. B. 1995, *VizieR Online Data Catalog*, 330, 50960
- Comito, C., Schilke, P., Phillips, T. G., et al. 2005, *ApJS*, 156, 127
- Daly, A. M., Bermúdez, C., López, A., et al. 2013, *ApJ*, 768, 81
- Demyk, K., Bottinelli, S., Caux, E., et al. 2010, *A&A*, 517, A17
- Esplugues, G. B., Tercero, B., Cernicharo, J., et al. 2013a, *A&A*, 556, A143
- Esplugues, G. B., Cernicharo, J., Viti, S. et al. 2013b, *A&A* 559, 51
- Fich, M., Johnstone, D., van Kempen, T. A., et al. 2010, *A&A*, 518, L86
- Fuente, A., Neri, R., Martín-Pintado, J., et al. 2001, *A&A*, 366, 873
- Fuente, A., Rizzo, J. R., Caselli, P., Bachiller, R., & Henkel, C. 2005b, *A&A*, 433, 535
- Fuente, A., Neri, R., & Caselli, P. 2005a, *A&A*, 444, 481 (FU05)
- Fuente, A., Castro-Carrizo, A., Alonso-Albi, T., et al. 2009, *A&A*, 507, 1475
- Fuente, A., Caselli, P., McCoey, C., et al. 2012, *A&A*, 540, A75
- Halfen, D. T., Apponi, A. J., Woolf, N., Polt, R., & Ziurys, L. M. 2006, *ApJ*, 639, 237
- Haykal, I., Carvajal, M., Tercero, B. et al., 2013, *A&A*, accepted
- Hollis, J. M., Lovas, F. J., & Jewell, P. R. 2000, *ApJ*, 540, L107
- Johnstone, D., Fich, M., McCoey, C., et al. 2010, *A&A*, 521, L41
- Kahane, C., Ceccarelli, C., Faure, A., & Caux, E. 2013, *ApJ*, 763, L38
- Kolesniková et al., 2014, *ApJ*, in press (arXiv:1401.7810)
- Jørgensen, J. K., Bourke, T. L., Myers, P. C., et al. 2005, *ApJ*, 632, 973
- Jørgensen, J. K., Bourke, T. L., Myers, P. C., et al. 2007, *ApJ*, 659, 479
- Loïnard, L., Castets, A., Ceccarelli, C., et al. 2003, *SFChem 2002: Chemistry as a Diagnostic of Star Formation*, 351
- López, A., Tercero, B., Kisiel, Z. et al., submitted to *A&A*
- Marcelino, N., Cernicharo, J., Tercero, B., & Roueff, E. 2009, *ApJ*, 690, L27
- Margulès, L., Huet, T. R., Demaison, J., et al. 2010, *ApJ*, 714, 1120
- Milam, S. N., Savage, C., Brewster, M. A., Ziurys, L. M., & Wyckoff, S. 2005, *ApJ*, 634, 1126
- Motiyenko, R. A., Tercero, B., Cernicharo, J., & Margulès, L. 2012, *A&A*, 548, A71
- Müller, H. S. P., Thorwirth, S., Roth, D. A., & Winnewisser, G. 2001, *A&A*, 370, L49
- Müller, H. S. P., Schlöder, F., Stutzki, J., & Winnewisser, G. 2005, *Journal of Molecular Structure*, 742, 215
- Neill, J. L., Crockett, N. R., Bergin, E. A., Pearson, J. C., & Xu, L.-H. 2013, *ApJ*, 777, 85
- Neri, R., Fuente, A., Ceccarelli, C., et al. 2007, *A&A*, 468, L33
- Palau, A., Fuente, A., Girart, J. M., et al. 2011, *ApJ*, 743, L32
- Palau, A., Fuente, A., Girart, J. M., et al. 2013, *ApJ*, 762, 120
- Parise, B., Castets, A., Herbst, E., et al. 2004, *A&A*, 416, 159
- Peng, T.-C., Despois, D., Brouillet, N., et al. 2013, *A&A*, 554, A78
- Pickett, H. M. 1991, *J. Molec. Spectroscopy* 148, 371
- Pickett, H. M., Poynter, R. L., Cohen, E. A., et al. 1998, *Journal of Quantitative Spectroscopy and Radiative Transfer*, 60, 883
- Pineda, J. E., Maury, A. J., Fuller, G. A., et al. 2012, *A&A*, 544, L7
- Öberg, K. I., van der Marel, N., Kristensen, L. E., & van Dishoeck, E. F. 2011, *ApJ*, 740, 14
- Requena-Torres, M. A., Martín-Pintado, J., Martín, S., & Morris, M. R. 2008, *ApJ*, 672, 352
- Sánchez-Monge, Á., Palau, A., Estalella, R., et al. 2010, *ApJ*, 721, L107
- Shevchenko, V. S., & Yakubov, S. D. 1989, *Soviet Ast.*, 33, 370
- Taquet, V., Ceccarelli, C., & Kahane, C. 2012, *A&A*, 538, A42
- Tercero, B., Cernicharo, J., Pardo, J. R., & Goicoechea, J. R. 2010, *A&A*, 517, A96
- Tercero, B., Vincent, L., Cernicharo, J., Viti, S., & Marcelino, N. 2011, *A&A*, 528, A26
- Tercero, B., Kleiner, I., Cernicharo, J., et al. 2013, *ApJ*, 770, L13
- Turner, B. E. 1990, *ApJ*, 362, L29
- Turner, B. E. 1991, *ApJS*, 76, 617
- Vastel, C., Phillips, T. G., Ceccarelli, C., & Pearson, J. 2003, *ApJ*, 593, L97
- Zapata, L. A., Loïnard, L., Rodríguez, L. F., et al. 2013, *ApJ*, 764, L14

Appendix A: Tables and Figures

Table A.1. Line identifications

Freq (MHz)	Molecular lines ¹	Comments ²
218132	EE-(CH ₃) ₂ CO 20 _{2,18} -19 _{3,17} , 20 _{3,18} -19 _{3,17} , 20 _{2,18} -19 _{2,17} , 20 _{3,18} -19 _{2,17} , aGg'-(CH ₂ OH) ₂ , HCOOH	
218143	U	
218157	U	
218163	AA-(CH ₃) ₂ CO 20 _{2,18} -19 _{3,17} , CH ₂ OHCHO	
218181	aGg'-(CH ₂ OH) ₂ 18 _{4,0} -18 _{3,1} , 18 _{5,0} -18 _{4,1}	
218199	O ¹³ CS 18-17	
218222	p-H ₂ CO 3 _{0,3} -2 _{0,2}	
218238	aGg'-(CH ₂ OH) ₂ 22 _{17,5} -21 _{17,4} , 22 _{17,6} -21 _{17,5}	
218259	A-CH ₃ OCHO 31 _{9,23} -31 _{8,24} , CH ₂ OHCHO	
218282	E-CH ₃ OCHO 17 _{-3,14} -16 _{-3,13}	
218298	A-CH ₃ OCHO 17 _{3,13} -16 _{3,13}	
218316	CH ₂ DOH 5 _{2,4} -5 _{1,5}	
218324	HC ₃ N 24-23, CH ₂ OHCHO	
218336	U	
218371	aGg'-(CH ₂ OH) ₂ 22 _{4,19} -21 _{4,18}	
218380	aGg'-(CH ₂ OH) ₂ 22 _{15,7} -21 _{15,6} , 22 _{15,8} -21 _{15,7}	
218389	CH ₃ CH ₂ CN 24 _{3,21} -23 _{3,20} , CH ₃ OCOD	
218404	A-CH ₂ DOCOH 18 _{5,14} -17 _{5,13} , S-CH ₂ DOCOH, CH ₃ OCOD	
218440	E-CH ₃ OH 4 ₂ -3 ₁	
218460	NH ₂ CHO 10 _{1,9} -9 _{1,8} , T-CH ₃ CH ₂ OH	
218475	p-H ₂ CO 3 _{2,2} -2 _{2,1}	
218493	CH ₃ OCH ₃ 23 _{3,21} -23 _{2,22}	
218519	E-CH ₃ OCOD 18 _{6,13} -17 _{6,12}	
218526	A-CH ₃ OCOD 18 _{6,13} -17 _{6,12}	
218541	HCOOD 10 _{3,7} -9 _{3,6}	
218554	T-CH ₃ CH ₂ OH 21 _{5,16} -21 _{4,17}	
218576	aGg'-(CH ₂ OH) ₂ 22 _{13,10} -21 _{13,9} , 22 _{13,9} -21 _{13,8}	
218585	A-CH ₃ OCHO 36 _{9,28} -36 _{8,29}	
218594	A-CH ₃ OCHO 27 _{7,21} -27 _{5,22}	
218611	U	
218632	EE-(CH ₃) ₂ CO 12 _{9,4} -11 _{8,3} , CH ₃ OCHO 27 _{7,21} -27 _{-5,22}	
218655	T-CH ₃ CH ₂ OH 7 _{2,5} -6 _{1,6} , CH ₃ OCHO $\nu_t=1$	
218672	A-CH ₃ CHO $\nu_t=1$ 28 _{7,22} -28 _{5,23}	
218681	E-CH ₃ CHO $\nu_t=1$ 33 _{-9,25} -33 _{-8,26}	
218688	CH ₂ DOH 17 _{4,13} -16 _{5,12}	
218696	CH ₂ DOH 17 _{4,14} -16 _{5,11}	
218707	aGg'-(CH ₂ OH) ₂ 22 _{12,10} -21 _{12,9} , 22 _{12,11} -21 _{12,10}	
218730	S-CH ₂ DOCOH 19 _{4,16} -18 _{4,15} , wing of C ₃ H ₂ 6 _{0,6} -5 _{1,5} ?	
218738	CH ₃ CH ₂ CN $\nu_{13}=1$ / $\nu_{21}=1$ 24 _{3,22} -23 _{3,21} , 24 _{3,21} -23 _{3,20} , CH ₃ CHO $\nu_t=1$	
218760	p-H ₂ CO 3 _{2,1} -2 _{2,0}	
218774	AE-(CH ₃) ₂ CO 12 _{9,4} -11 _{8,3}	
218782	U	
218796	CH ₂ DOH 20 _{1,20} -19 _{2,17} , G-CH ₃ CH ₂ OH, CH ₃ OCOD	
218815	E-CH ₃ OH $\nu_t=2$ 16 ₋₈ -15 ₋₉ , AA-(CH ₃) ₂ CO	
218830	E-CH ₃ OCHO $\nu_t=1$ 18 _{13,5} -17 _{13,4}	
218850	U	
218860	HC ₃ N $\nu_7=1$ 24 ₋₁ -23 ₋₁	
218873	aGg'-(CH ₂ OH) ₂ 22 _{11,12} -21 _{11,11} , 22 _{11,11} -21 _{11,10}	
218903	OCS 18-17	
218914	U	
218922	U	
218938	HCOOH 8 _{1,8} -7 _{0,7}	
218955	A- ¹³ CH ₃ OCHO 40 _{8,33} -39 _{9,30}	
218967	E-CH ₃ OCHO $\nu_t=1$ 18 _{12,6} -17 _{12,5} , CH ₂ OHCHO, CH ₂ DOCOH, ¹³ CH ₃ OCHO	
218980	HNCO 10 _{1,10} -9 _{1,9} , HN ¹³ CO	
219007	S-CH ₂ DOCOH 32 _{9,23} -32 _{8,24}	
219019	S-CH ₂ DCH ₂ CN 27 _{1,27} -26 _{1,26}	
219037	CH ₂ OHCHO 39 _{10,30} -39 _{9,31}	

Continued on next page

Freq (MHz)	Molecular lines ¹	Comments ²
219067	CH ₂ OHCHO _{27,25-27,26,27,25-27,12,6} , CH ₃ OCHO $\nu_t=1$, ¹³ CH ₃ OCHO, CH ₂ DCH ₂ CN	
219078	E-CH ₃ OCHO $\nu_t=1$ 28 _{3,25-28,2,26} , AE-(CH ₃) ₂ CO, EA-(CH ₃) ₂ CO	
219090	aGg ⁺ -(CH ₂ OH) ₂ 22 _{10,13-21,10,12,22,10,12-21,10,11} , CH ₃ OCHO	
219098	A-CH ₂ DOCOH 18 _{6,12-17,6,11} , ¹³ CH ₃ OCHO, CH ₂ OHCHO, HCOOH	
219108	A-CH ₃ OCHO 34 _{7,28-34,5,29}	
219115	U	
219123	CH ₂ OHCHO 29 _{3,26-29,2,27}	
219132	S-CH ₂ DOCOH 19 _{8,12-18,8,11,19,8,11-18,8,10}	
219143	U	
219154	A-CH ₃ OCHO $\nu_t=1$ 18 _{11,7-17,11,6} , 10 _{4,6-9,3,6}	
219171	OCS $\nu_2=1$ 18 _{-1-17,-1} , T-CH ₃ CH ₂ OH, HC ₃ N $\nu_7=1$	
219188	EE-(CH ₃) ₂ CO 5 _{5,1-5,4,1}	
219196	U	
219204	CH ₂ DOH 20 _{5,16-19,6,13,20,5,15-19,6,14}	
219220	AE-(CH ₃) ₂ CO 21 _{1,20-20,2,19,21,2,20-20,1,19} , EA-(CH ₃) ₂ CO, CH ₃ CH ₂ CN $\nu_{13}/\nu_{21}=1$	
219228	CH ₂ OHCHO 31 _{5,27-31,3,28}	
219242	A-CH ₃ OCOD 21 _{0,21-20,1,20,21,1,21-20,1,20,21,0,21-20,0,20,21,1,21-20,0,20} , EE-(CH ₃) ₂ CO	
219264	AA-(CH ₃) ₂ CO 21 _{1,20-20,2,19,21,2,20-20,1,19} , CH ₃ OCHO	
219276	SO ₂ 22 _{7,15-23,6,18}	
219295	S-CH ₂ DCH ₂ CN 26 _{3,24-25,3,23} , CH ₃ CHO	
219305	CH ₃ OCH ₃ 31 _{6,26-30,7,23} , CH ₂ OHCHO	
219311	AA-(CH ₃) ₂ CO 12 _{9,4-11,8,3}	
219321	CH ₃ CH ₂ CN $\nu_{13}=1/\nu_{21}=1$ 25 _{1,25-24,1,24,25,2,25-24,2,23} , CH ₃ OCHO $\nu_t=1$	
219330	E-CH ₃ OCHO $\nu_t=1$ 18 _{-15,4-17,-15,3}	
219341	H ¹³ COOH 10 _{0,10-9,0,9}	
219355	³⁴ SO ₂ 11 _{1,10-10,0,10}	
219370	S-CH ₂ DCH ₂ CN 26 _{12,14-25,12,13,26,12,15-25,12,14}	
219386	aGg ⁺ -(CH ₂ OH) ₂ 22 _{9,14-21,9,13,22,9,13-21,9,12}	
219389	U	
219398	OCS $\nu_2=1$ 18-17	
219411	E-CH ₃ OCHO $\nu_t=1$ 18 _{0,8-17,0,7}	
219441	U	
219467	CH ₃ OCH ₃ 28 _{5,24-27,6,21} , CH ₃ CH ₂ CN, AE-(CH ₃) ₂ CO, EA-(CH ₃) ₂ CO	
219479	CH ₃ OCHO $\nu_t=1$ 18 _{-14,5-17,-14,4} , CH ₃ OCHO	
219490	DC ₃ N 26-25	
219506	CH ₃ CH ₂ CN 24 _{2,22-23,2,21}	
219512	U	
219541	aGg ⁺ -(CH ₂ OH) ₂ 22 _{2,21-21,2,20}	
219550	HNCO 10 _{4,6-9,4,5,10,4,7-9,4,6} , CH ₃ OH	Partially overlapped with C ¹⁸ O
219560	C ¹⁸ O 2-1	Partially overlapped with C ¹⁸ O
219570	A-CH ₃ OCHO $\nu_t=1$ 18 _{15,4-17,15,3,18,15,3-17,15,2,18,16,2-17,16,1,18,16,3-17,16,2}	
219580	aGg ⁺ -(CH ₂ OH) ₂ 22 _{1,21-21,1,20} , CH ₃ OCHO	
219584	A-CH ₃ OCHO $\nu_t=1$ 18 _{13,6-17,13,5,18,13,5-17,13,4} , CH ₃ OCHO	
219593	E-CH ₃ OCHO 28 _{-9,19-28,-8,20} , CH ₃ OCOD, CH ₂ OHCHO	
219600	E-CH ₃ OCHO 30 _{9,22-30,8,23}	
219607	E-CH ₃ OCHO 30 _{5,26-30,-3,27} , EE-(CH ₃) ₂ CO	
219622	A-CH ₃ OCHO $\nu_t=1$ 18 _{12,6-17,12,5,18,12,7-17,12,6}	
219642	E-CH ₃ OCHO $\nu_t=1$ 18 _{-13,6-17,-13,5}	
219657	HNCO 10 _{3,7-9,3,6} , HN ¹³ CO	
219674	A-CH ₃ OCHO 30 _{5,26-30,3,27}	
219696	A-CH ₃ OCHO $\nu_t=1$ 18 _{11,8-17,11,7,18,11,7-17,11,6}	
219705	A-CH ₃ OCHO $\nu_t=1$ 18 _{4,15-17,4,14}	
219720	E-CH ₃ OCHO $\nu_t=1$ 32 _{-9,24-32,-8,25,28,-4,25-28,2,26}	
219735	HNCO 10 _{2,9-9,2,8,10,2,8-9,2,7} , HN ¹³ CO	
219751	AA-(CH ₃) ₂ CO 33 _{8,25-33,3,26,33,9,25-33,7,26}	
219764	E-CH ₃ OCHO $\nu_t=1$ 18 _{9,9-17,9,8} , aGg ⁺ -(CH ₂ OH) ₂ 20 _{4,16-19,4,15}	
219780	A-CH ₃ CHO $\nu_t=2$ 11 _{1,10-10,1,9} , CH ₃ OCHO $\nu_t=1$	
219798	HNCO 10 _{1,10-9,0,9}	
219804	aGg ⁺ -(CH ₂ OH) ₂ 22 _{8,15-21,8,14} , HN ¹³ CO	

Continued on next page

Freq (MHz)	Molecular lines ¹	Comments ²
219823	A-CH ₃ OCHO $\nu_t=1$ 18 _{10,9} -17 _{10,8} , 18 _{10,8} -17 _{10,7} , AE-(CH ₃) ₂ CO, EA-(CH ₃) ₂ CO, CH ₃ CHO	
219863	U	
219876	U	
219894	U	
219900	U	CH ₂ CHCN 10 _{2,9} -9 _{1,8}
219908	o-H ₂ ¹³ CO 3 _{1,2} -2 _{1,1}	
219916	U	E-CD ₃ CN 14 ₅ -13 ₅
219949	SO 5 ₆ -4 ₅	
219965	U	A-CD ₃ CN 14 ₃ -13 ₃
219980	U	E-CD ₃ CN 14 ₂ -13 ₂
219991	U	A-CD ₃ CN 14 ₀ -13 ₀
220030	CH ₃ OCHO $\nu_t=1$ 18 _{9,10} -17 _{9,9} , 18 _{9,9} -17 _{9,8}	
220037	HCOOH 10 _{0,10} -9 _{0,9} , CH ₃ OCHO $\nu_t=1$	
220054	CH ₂ OHCHO 35 _{10,26} -35 _{9,27} ,	
220077	E-CH ₃ OH 8 _{0,8} -7 _{1,6} , CH ₂ DOH	
220094	aGg'-(CH ₂ OH) ₂ 24 _{11,13} -24 _{10,15} , 24 _{11,14} -24 _{10,14}	
220140	U	
220155	T-CH ₃ CH ₂ OH 24 _{3,22} -24 _{2,23}	
220167	E-CH ₃ OCHO 17 _{-4,13} -16 _{-4,12} , AA-(CH ₃) ₂ CO	
220178	o-H ₂ CCO 11 _{1,11} -10 _{1,10}	
220190	A-CH ₃ OCHO 17 _{4,13} -16 _{4,12}	
220196	CH ₂ OHCHO 7 _{6,2} -6 _{5,1} , 7 _{6,1} -6 _{5,2}	
220203	CH ₂ OHCHO 11 _{4,7} -10 _{3,8}	
220225	U	
220235	E-CH ₃ CN 12 ₁₁ -11 ₁₁	
220243	U	
220258	E-CH ₃ OCHO $\nu_t=1$ 18 _{8,10} -17 _{8,9} , CH ₂ DOCOH	
220270	U	
220279	U	
220300	A-CH ₂ DOCOH 20 _{1,19} -19 _{1,18} , CH ₃ ¹³ CN	
220307	E-CH ₃ OCHO $\nu_t=1$ 18 _{-10,9} -17 _{-10,8}	
220321	A- ¹³ CH ₃ OH 17 _{7,11} -18 _{6,12} , 17 _{7,10} -18 _{6,13} , CH ₃ CN	
220332	U	
220345	U	CH ₂ CHCN 9 _{4,5} -10 _{3,8} , G+CH ₃ CH ₂ OH CH ₂ DOCOH
220355	AE-(CH ₃) ₂ CO 22 _{1,22} -21 _{1,21} , 22 _{0,22} -21 _{0,21} , EA-(CH ₃) ₂ CO	
220361	EE-(CH ₃) ₂ CO 22 _{0,22} -21 _{1,21} , 22 _{1,22} -21 _{1,21} , 22 _{1,22} -21 _{0,21} , 22 _{0,22} -21 _{0,21}	
220368	A-CH ₃ OCHO $\nu_t=1$ 18 _{8,11} -17 _{8,10} , 18 _{8,10} -17 _{8,9} , AA-(CH ₃) ₂ CO, EA-(CH ₃) ₂ CO	
220390	H ¹³ CC ₂ N 25-24	Partially blended with ¹³ CO
220398	¹³ CO 2-1, CH ₃ OH	
220403	A-CH ₃ CN 12 ₉ -11 ₉ , aGg'-(CH ₂ OH) ₂	Partially blended with ¹³ CO
220409	E-CH ₃ OCHO $\nu_t=1$ 18 _{-4,15} -17 _{-4,14}	Partially blended with ¹³ CO
220417	A-CH ₃ OCHO $\nu_t=1$ 18 _{3,16} -17 _{2,15}	
220427	U	
220446	A-CH ₃ CHO 21 _{4,18} -22 _{1,21}	
220466	CH ₂ OHCHO 20 _{2,18} -19 _{3,17} , AE-(CH ₃) ₂ CO	
220476	E-CH ₃ CN 12 ₈ -11 ₈	
220486	A-CH ₃ ¹³ CN 12 ₆ -11 ₆	
220498	aGg'-(CH ₂ OH) ₂ 22 _{7,15} -21 _{7,14}	
220504	³³ SO ₂ 27 ₁ -27 ₂₈ , 27 ₁ -27 ₂₇	
220525	A-CH ₃ OCHO $\nu_t=1$ 10 _{4,6} -9 _{3,7}	
220532	E-CH ₃ ¹³ CN 12 ₅ -11 ₅	
220540	E-CH ₃ CN 12 ₇ -11 ₇	
220551	CH ₂ DOH 17 _{1,16} -17 _{0,17}	
220570	E-CH ₃ ¹³ CN 21 _{4,18} -22 _{1,21}	
220585	HNCO 10 _{1,9} -9 _{1,8}	
220595	A-CH ₃ CN 12 ₆ -11 ₆	
220602	T-CH ₃ CH ₂ OH 13 _{1,13} -12 _{0,12}	
220606	E-CH ₃ OCHO $\nu=1$ 18 _{-3,16} -17 _{2,15}	
220622	E-CH ₃ ¹³ CN 12 ₂ -11 ₂	

Continued on next page

Freq (MHz)	Molecular lines ¹	Comments ²
220640	E-CH ₃ CN 12 ₅ -11 ₅	CH ₂ CHCN $\nu=1$ 10 _{3,7} -10 _{2,8}
220647	E-CH ₃ OCHO $\nu_t=1$ 18 _{-9,10} -17 _{-9,9}	
220662	CH ₃ CH ₂ CN 25 _{2,24} -24 _{2,23} , EE-(CH ₃) ₂ CO	
220679	E-CH ₃ CN 12 ₄ -11 ₄	
220695	AE-(CH ₃) ₂ CO 29 _{5,25} -29 _{4,26} , 29 _{4,25} -29 _{3,26}	
220701	CH ₂ OHCHO 40 _{9,32} -40 _{8,33}	
220709	A-CH ₃ CN 12 ₃ -11 ₃	
220730	E-CH ₃ CN 12 ₂ -11 ₂	
220745	A-CH ₃ CN 12 ₀ -11 ₀ , E-CH ₃ CN 12 ₁ -11 ₁	
220764	EE-(CH ₃) ₂ CO 11 _{11,9} -10 _{10,0}	
220785	E-CH ₃ OCHO 28 _{-3,25} -28 _{3,26} , CH ₃ OCHO $\nu_t=1$	
220793	U	
220814	E-CH ₃ OCHO 28 _{-3,25} -28 _{-2,26}	
220847	CH ₃ OCH ₃ 24 _{4,20} -23 _{5,19}	
220857	U	
220866	CH ₃ OCHO $\nu_t=1$ 19 _{2,17} -18 _{3,16} , CH ₃ OCHO, G-CH ₃ CH ₂ OH, CH ₃ CHO $\nu_t=1$	
220887	A-CH ₃ OCHO 18 _{17,1} -17 _{17,0} , 18 _{17,2} -17 _{17,1}	
220892	CH ₃ OCH ₃ 23 _{4,20} -23 _{3,21} , CH ₃ OCHO	
220901	E-CH ₃ OCHO 18 _{-17,1} -17 _{-17,0}	
220913	CH ₃ OCHO $\nu_t=1$ 18 _{7,12} -17 _{7,11} , CH ₃ OCHO	
220926	A-CH ₃ OCHO 18 _{16,3} -17 _{16,2} , 18 _{16,2} -17 _{16,1} , CH ₂ DOCOH, AE-(CH ₃) ₂ CO, EA-(CH ₃) ₂ CO	
220936	E-CH ₃ OCHO 18 _{-16,2} -17 _{-16,1}	
220946	A-CH ₃ OCHO $\nu=1$ 18 _{7,11} -17 _{7,10} , CH ₃ OCHO	
220961	AA-(CH ₃) ₂ CO 11 _{11,1} -10 _{10,0} , 11 _{11,0} -10 _{10,1} , CH ₃ OCHO, CH ₃ NC	
220978	A-CH ₃ OCHO 18 _{15,4} -17 _{15,3} , 18 _{15,3} -17 _{15,2} , CH ₃ CN $\nu_8=1$, EE-(CH ₃) ₂ CO	
220985	E-CH ₃ OCHO $\nu_t=1$ 18 _{7,11} -17 _{7,10} , CH ₃ OCHO	
220989	S-CH ₂ DOCOH 19 _{6,13} -18 _{6,12}	
220999	G-CH ₃ CH ₂ OH 13 _{0,13} -12 _{0,12} , CH ₃ OCHO	
221008	aGg'-(CH ₂ OH) ₂ 21 _{4,18} -20 _{4,17} , CH ₂ OHCHO	
221013	E-CH ₃ NC 11 ₅ -10 ₅	
221026	A-CH ₃ OCHO 36 _{6,30} -36 _{5,31}	
221038	aGg'-(CH ₂ OH) ₂ 22 _{6,17} -21 _{6,16}	
221049	A-CH ₃ OCHO 18 _{14,5} -17 _{14,4} , 18 _{14,4} -17 _{14,3}	
221059	CH ₃ CN $\nu_8=1$ 12 _{8,1} -11 _{8,1} , CH ₃ NC	
221066	E-CH ₃ OCHO 37 _{9,29} -37 _{8,30}	
221077	A-CH ₃ OCHO 29 _{9,21} -29 _{8,22} , CH ₃ CN $\nu_8=1$	
221087	E-CH ₃ OCHO 29 _{9,21} -29 _{8,22}	
221092	A-CH ₃ NC 11 ₃ -10 ₃	
221100	aGg'-(CH ₂ OH) ₂ 22 _{5,18} -21 _{5,17}	
221112	E-CH ₃ OCHO $\nu_t=1$ 18 _{-8,11} -17 _{-8,10} , ³⁴ SO ₂	
221119	E-CH ₃ NC 11 ₂ -10 ₂	
221132	E-CH ₃ NC 11 ₁ -10 ₁ , CH ₃ CN $\nu_8=1$, CH ₃ OCHO $\nu_t=1$	
221138	A-CH ₃ NC 11 ₀ -10 ₀	
221141	A-CH ₃ OCHO 18 _{13,6} -17 _{13,5} , 18 _{13,5} -17 _{13,4} , E-CH ₃ OCHO 18 _{-13,5} -17 _{-13,4}	
221157	E-CH ₃ OCHO 18 _{13,6} -17 _{13,5} , CH ₂ DOH, CH ₃ OCOD	
221165	A-CH ₃ OCHO $\nu=1$ 37 _{8,30} -37 _{7,31}	
221178	CH ₂ DOH 6 _{2,5} -6 _{1,6} , HDCS 7 _{1,6} -6 _{1,5}	
221191	p-D ₂ CO 4 _{1,4} -3 _{1,3}	
221198	CH ₃ OCH ₃ 27 _{5,22} -27 _{4,23} , CH ₃ CN $\nu_8=1$	
221210	CH ₃ CN $\nu_8=1$ 12 _{8,2} -11 _{8,2}	
221216	E-CH ₃ CHO $\nu_t=2$ 11 _{2,10} -10 _{2,9}	
221222	A-CH ₃ CHO $\nu_t=1$ 22 _{1,21} -22 _{0,22}	
221253	CH ₃ CN $\nu_8=1$ 12 _{5,1} -11 _{5,1}	
221266	A-CH ₃ OCHO 18 _{12,7} -17 _{12,6} , 18 _{12,6} -17 _{12,5} , CH ₃ CN $\nu_8=1$ 12 _{7,2} -11 _{7,2}	
221273	CH ₂ DOH 5 _{1,5} -4 _{1,4}	
221285	E- ¹³ CH ₃ OH 8 _{-1,8} -7 _{0,7} , CH ₃ OCHO	
221298	A-CH ₃ CHO 13 _{3,10} -13 _{2,11} , CH ₃ CN $\nu_8=1$ 12 _{4,1} -11 _{4,1} , CH ₃ OCHO	
221312	CH ₃ CN $\nu_8=1$ 12 _{6,2} -11 _{6,2} , NH ₂ CHO	
221326	U	
221338	aGg'-(CH ₂ OH) ₂ 23 _{3,21} -22 _{3,20} , CH ₃ CN $\nu_8=1$ 12 _{3,1} -11 _{3,1} , aGg'-(CH ₂ OH) ₂	
221350	CH ₃ CN $\nu_8=1$ 12 _{5,2} -11 _{5,2}	

Continued on next page

Freq (MHz)	Molecular lines ¹	Comments ²
221367	CH ₃ CN $\nu_8=1$ 12 _{2,1} -11 _{2,1}	
221382	CH ₃ CN $\nu_8=1$ 12 _{4,2} -11 _{4,2}	
221392	CH ₂ DOH 10 _{1,10} -9 _{0,9} , CH ₃ CN $\nu_8=1$ 12 _{1,1} -11 _{1,1}	
221404	CH ₃ CN $\nu_8=1$ 12 _{3,2} -11 _{3,2} , CH ₂ DOCOH, CH ₃ OCHO	
221423	A- ¹³ CH ₃ OH $\nu_t=1$ 6 _{1,6} - 7 _{2,5} , CH ₃ OCHO, CH ₃ CN $\nu_8=1$	
221433	A-CH ₃ OCHO 18 _{11,8} -17 _{11,7} , 18 _{11,7} -17 _{11,6} , CH ₃ CH ₂ CN $\nu_{13}/\nu_{21}=1$	
221445	E-CH ₃ OCHO 18 _{11,8} -17 _{11,7} , CH ₃ CH ₂ CN $\nu_{13}/\nu_{21}=1$	
221465	CH ₂ OHCHO 3 _{4,10,25} -3 _{4,9,26}	
221480	E-CH ₃ CHO $\nu_t=1$ 23 _{8,15} -24 _{7,17} , CH ₃ CHO $\nu_t=2$	
221494	aGg'-(CH ₂ OH) ₂ 12 _{5,8} -11 _{4,8}	
221500	EE-(CH ₃) ₂ CO 27 _{2,25} -27 _{2,26} , 27 _{2,25} -27 _{1,26} , 27 _{3,25} -27 _{2,26} , 27 _{3,25} -27 _{1,26}	
221519	U	
221526	EA-(CH ₃) ₂ CO 31 _{20,11} -31 _{17,14}	
221534	U	
221547	U	
221560	A-CH ₂ DOCOH 7 _{6,2} -6 _{5,1} , 7 _{6,1} -6 _{5,2} , S-CH ₂ DOCOH 21 _{3,18} -20 _{4,17} , 50 _{9,41} -50 _{8,42}	
221566	U	
221582	aGg'-(CH ₂ OH) ₂ 18 _{4,15} -17 _{3,14}	
221597	U	
221605	U	
221627	CH ₃ CN $\nu_8=1$ 12 _{1,2} -11 _{-1,2}	
221649	E-CH ₃ OCHO 18 _{-10,8} -17 _{-10,7}	
221660	A-CH ₃ OCHO 18 _{10,9} -17 _{10,8} , 18 _{10,8} -17 _{10,7} , E-CH ₃ OCHO 18 _{4,15} -17 _{4,14}	

¹ Lines are ordered from major to minor contribution to the total integrated flux according with our model.

² The lines in this column correspond to doubtful identifications.

Table A.2. Line identifications (FU05)

(MHz)	Molecular lines ¹	Comments ²
228140	G-CH ₃ CH ₂ OH 18 _{5,14} -18 _{4,15}	
228151	OC ³³ S 19-18	
228167	AE-(CH ₃) ₂ CO 34 _{9,26} -34 _{8,27} ,34 _{8,26} -34 _{7,27} , EA-(CH ₃) ₂ CO 34 _{9,26} -34 _{8,27} ,34 _{8,26} -34 _{7,27} , CH ₃ CH ₂ CN	
228186	U	
228199	HCOOH 21 _{6,16} -22 _{5,17}	
228211	CH ₃ OCHO $\nu_7=1$ 18 _{3,15} -17 _{3,14}	
228231	CH ₂ DOH 11 _{2,9} -11 _{1,10}	
228246	CH ₂ DOH 15 _{2,13} -15 _{1,14}	
228257	U	
228272	A-CH ₃ OCHO 24 _{9,16} -24 _{8,17} , S ¹⁸ O, CH ₃ OCOD	
228293	A-CH ₃ OCOD 18 _{4,14} -17 _{4,13}	
228307	HC ₃ N $\nu_7=1$ 25 ₁ -24 ₁ , EE-CH ₃ COCH ₃	
228336	U	CH ₂ CHCN 16 _{3,14} -16 _{2,15}
228359	E-CH ₃ OCHO 24 _{-9,15} -24 _{8,17} , CH ₃ OCHO $\nu_7=1$, CH ₂ DCH ₂ CN, aGg ⁻ -(CH ₂ OH) ₂	
224374	U	
228384	U	
228410	H ¹³ COOH 10 _{2,8} -9 _{2,7}	
228436	CH ₃ OCH ₃ 26 _{3,23} -25 _{4,21} , 26 _{3,24} -25 _{4,21}	
228439	A-CH ₂ DOCOH 19 _{9,10} -18 _{9,9} ,19 _{9,10} -18 _{9,10} ,19 _{9,11} -18 _{9,9} ,19 _{9,11} -18 _{9,10} , CH ₃ OCOD, HCOOH	
228448	A-CH ₃ OCOD 20 _{2,18} -19 _{2,17} , AA-(CH ₃) ₂ CO	
228464	E-CH ₃ OCOD 19 _{-9,10} -18 _{-9,9} , CH ₃ OCHO $\nu_7=1$	
228483	CH ₃ CH ₂ CN 25 _{2,23} -24 _{2,22} , CH ₃ OCOD	
228490	G+CH ₃ CH ₂ OH 8 _{5,3} -8 _{4,4} , 8 _{5,4} -8 _{4,5}	Undetected
228500	AE-(CH ₃) ₂ CO 12 _{10,3} -11 _{9,2}	
228512	G-CH ₃ CH ₂ OH 15 _{5,10} -15 _{4,11} , AE-(CH ₃) ₂ CO, EA-(CH ₃) ₂ CO	
228526	G-CH ₃ CH ₂ OH 17 _{5,13} -17 _{4,14}	
228544	HCOOH 10 _{2,8} -9 _{2,7}	
228559	G+CH ₃ CH ₂ OH 7 _{5,2} -7 _{4,3} , 7 _{5,3} -7 _{4,4}	Undetected
231060	OCS 19-18	
231077	U	OCS wing?, CH ₃ OCHO $\nu_7=1$
231102	U	
231114	E-CH ₃ CHO 9 _{3,6} -9 _{2,7}	
231127	aGg ⁻ -(CH ₂ OH) ₂ 23 _{7,16} -22 _{7,15}	
231144	o-H ₂ ¹³ CS 7 _{3,5} -6 _{3,4} ,7 _{3,4} -6 _{3,3} , CH ₃ OCHO $\nu_7=1$, CH ₃ CHO $\nu_7=1$	
231167	E-CH ₃ CHO 10 _{10,2} -11 _{10,1}	
231188	H ¹³ COOH 10 _{1,9} -9 _{1,8} , CH ₃ OCHO, CH ₃ CHO	contaminated with ¹³ CS wings?
231200	A-CH ₃ OCHO 21 _{9,12} -21 _{8,13} , E-CH ₃ OCHO 21 _{-9,12} -21 _{-8,13} , E-CH ₃ CHO	contaminated with ¹³ CS wings?
231220	¹³ CS 5-4	
231226	A-CH ₃ CHO 12 _{9,3} -11 _{9,2} ,12 _{9,4} -11 _{9,3} , E-CH ₃ CHO 12 _{7,5} -11 _{7,4}	
231232	A-CH ₃ CHO 12 _{8,4} -11 _{8,3} ,12 _{8,5} -11 _{8,4} , E-CH ₃ CHO 12 _{8,5} -11 _{8,4} , CH ₃ OCHO $\nu_7=1$	contaminated with ¹³ CS wings?
231245	A-CH ₃ CHO 12 _{7,6} -11 _{7,5} ,12 _{7,5} -11 _{7,4} , CH ₃ OCHO $\nu_7=1$	
231255	U	
231268	A-CH ₃ CHO 12 _{6,7} -11 _{6,6} ,12 _{6,6} -11 _{6,5} , E-CH ₃ CHO 12 _{7,6} -11 _{7,5}	
231280	A-CH ₃ OH 10 _{2,-1} -9 _{3,-1} , CH ₃ CHO	
231293	U	
231311	CH ₃ CH ₂ CN 26 _{1,25} -25 _{1,24} ,27 _{0,27} -26 _{1,26} ,24 _{2,23} -23 _{1,22} , CH ₃ CHO	
231329	A-CH ₃ CHO 12 _{5,8} -11 _{5,7} ,12 _{5,7} -11 _{5,6}	
231344	OCS $\nu_2=1$ 19 ₋₁ -18 ₋₁	
231369	E-CH ₃ CHO 12 _{5,7} -11 _{5,6} ,12 _{5,8} -11 _{5,7}	
231383	E-CH ₃ CHO $\nu=1$ 12 _{5,8} -11 _{5,7}	
231410	o-D ₂ CO 4 _{0,4} -3 _{0,3}	
231417	E-CH ₃ COOH $\nu=1$ 19 _{-16,4} -18 _{-16,3}	
231454	A-CH ₃ CHO 12 _{4,9} -11 _{4,8}	
231466	A-CH ₃ CHO 9 _{3,6} -9 _{2,7}	
231483	E-CH ₃ CHO 12 _{4,8} -11 _{4,7}	
231506	HCOOH 10 _{1,9} -9 _{1,8} , CH ₃ CHO	
231525?	aGg ⁻ -(CH ₂ OH) ₂ 23 _{6,18} -22 _{6,17}	
231533?	U	
231560	T-CH ₃ CH ₂ OH 20 _{5,16} -20 _{4,17}	

¹ Lines are ordered from major to minor contribution to the total integrated flux according with our model.² The lines in this column correspond to doubtful identifications.

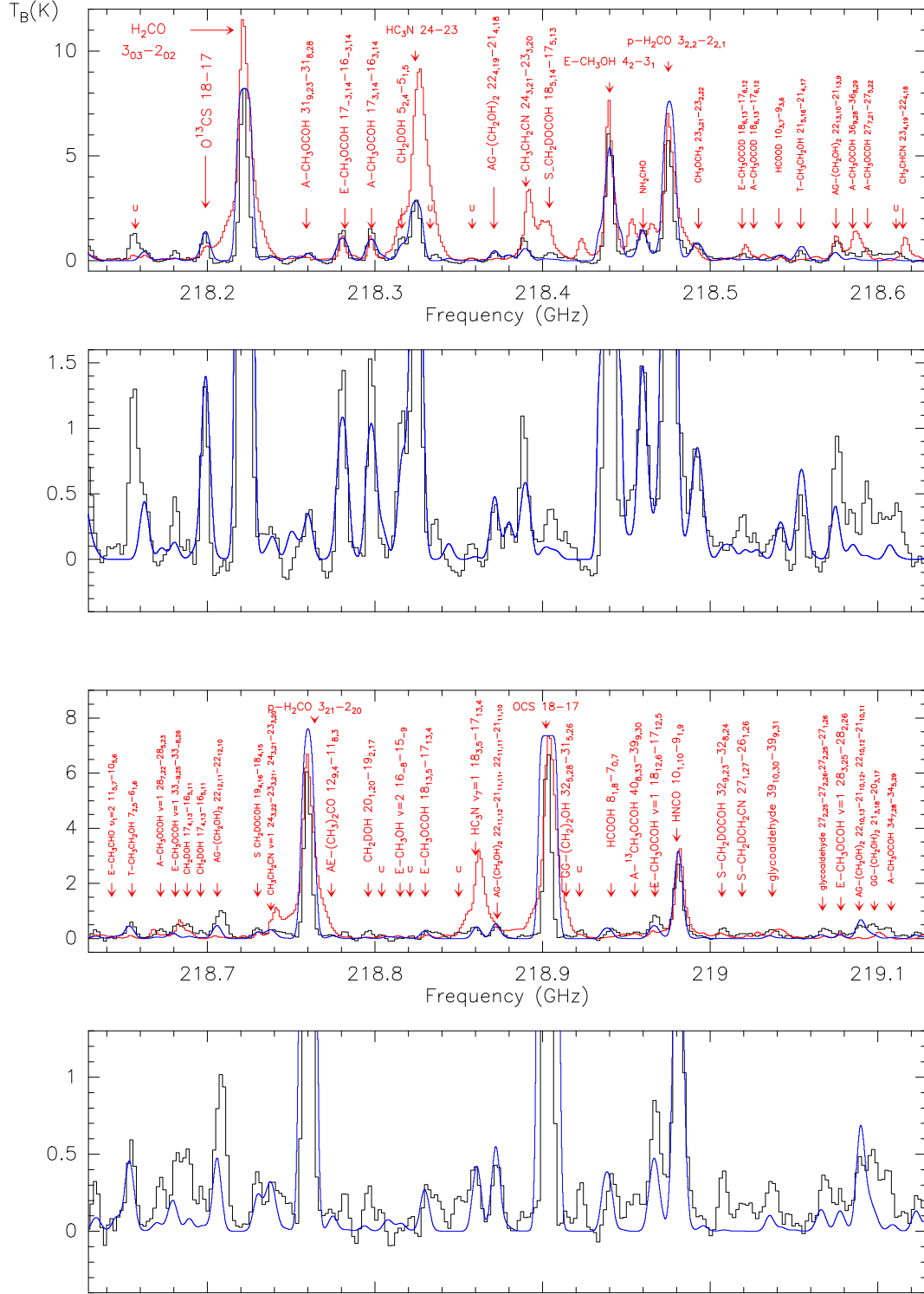


Fig. A.1. Comparison of the interferometric spectra towards NGC 7129 - FIRS 2 (black line) with the single-dish spectrum of Orion KL (red line). The Orion spectra have been provided by B. Tercero and J. Cernicharo and multiplied by a factor 0.43 for an easier comparison. The spectrum was observed towards: $5^{\text{h}}35^{\text{m}}14^{\text{s}}.5$, $-5^{\circ}22'30''.0$ (J2000) and is centered at a velocity of 7 km s^{-1} . Lines are labelled in red. When several lines are blended, only the most intense ones are indicated. In blue, the spectra synthesized with the parameters shown in Table 3. The intensity scale is brightness temperature.

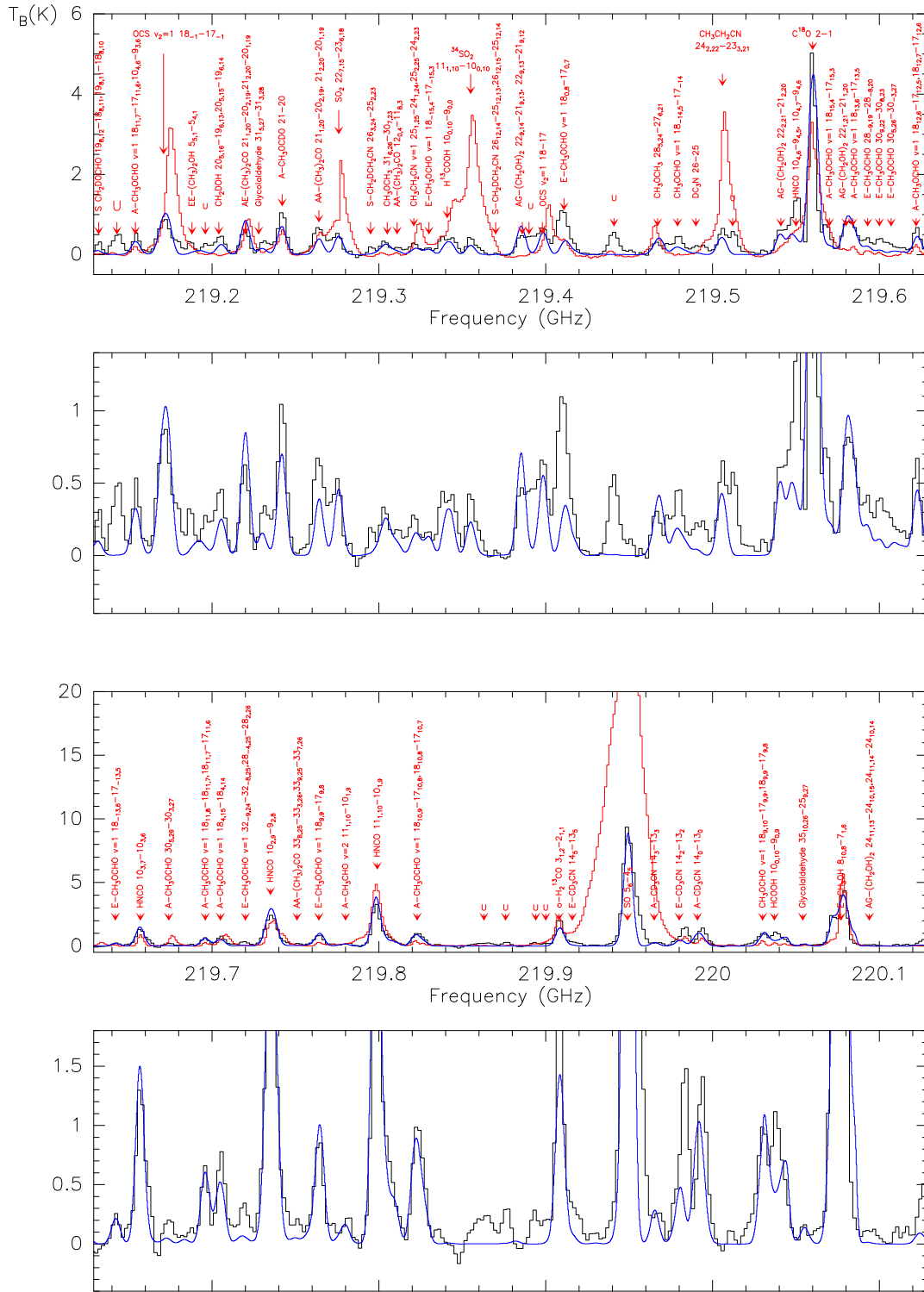


Fig. A.2. The same as Fig. A.1.

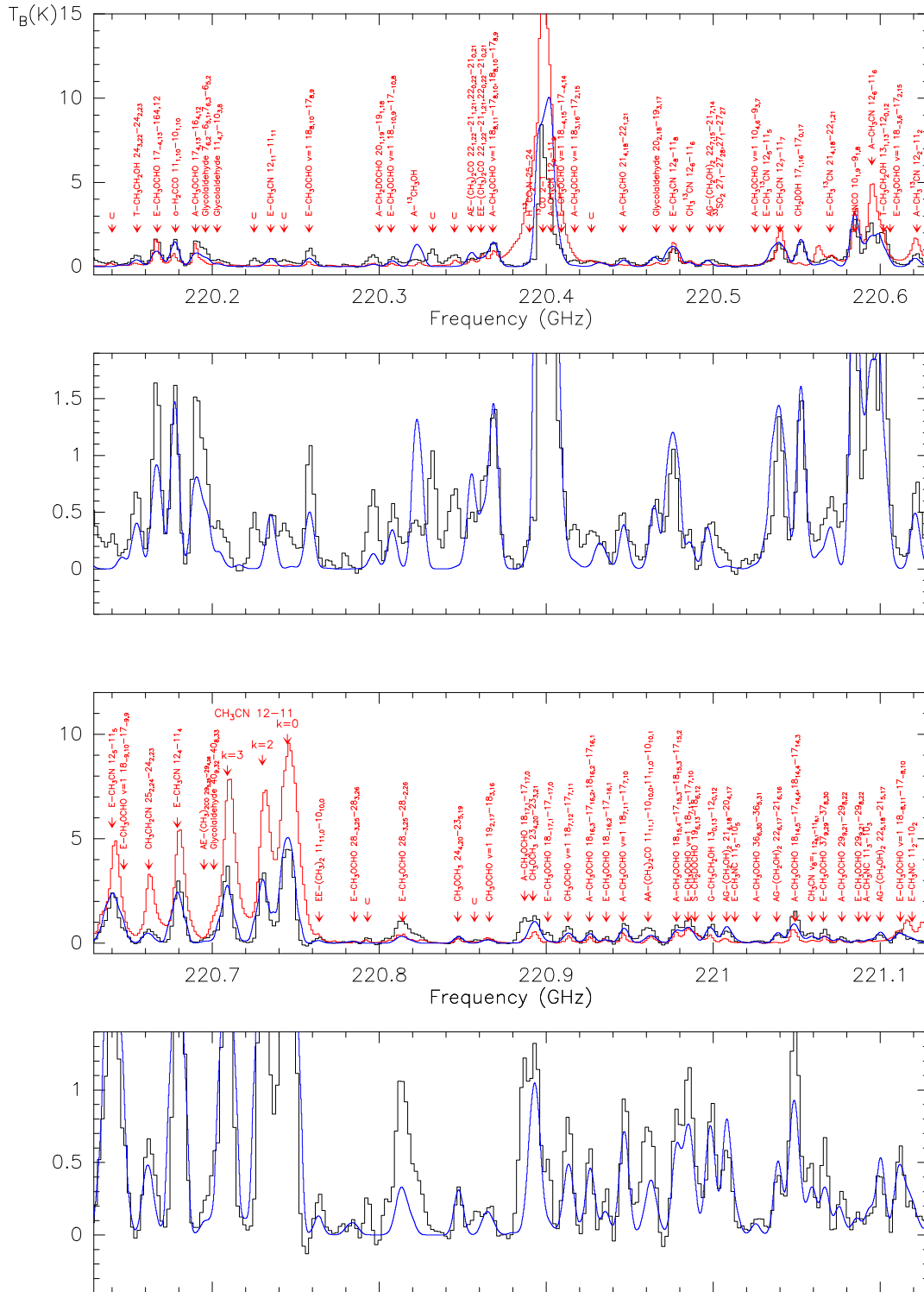


Fig. A.3. The same as Fig. A.1.

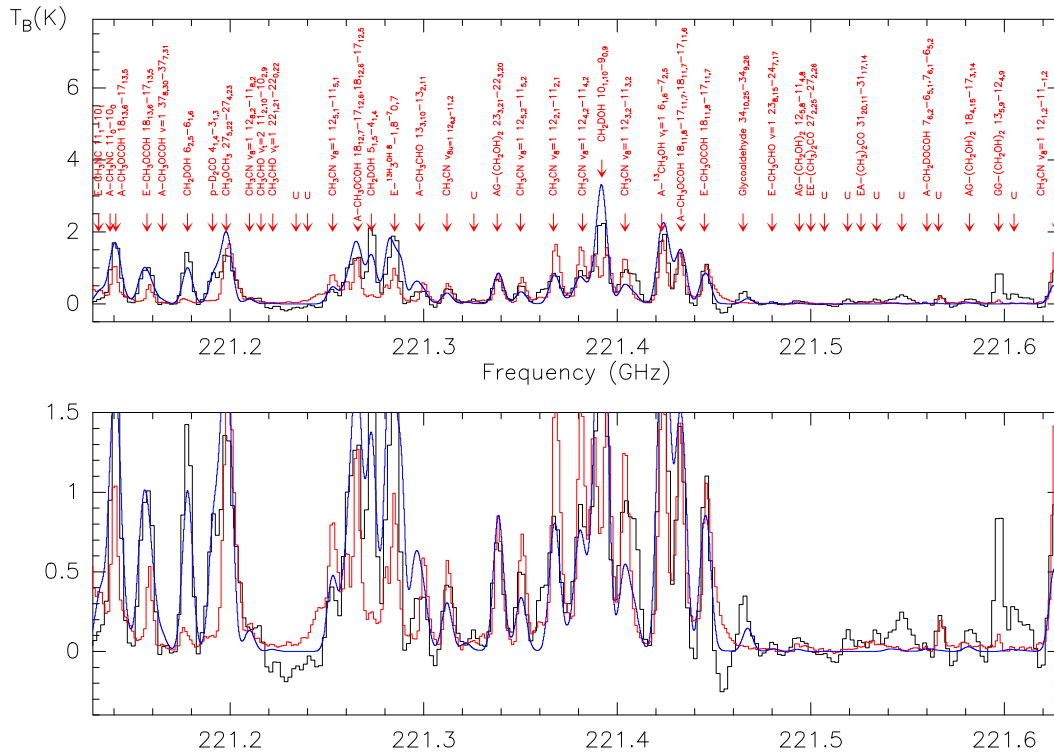


Fig. A.4. The same as Fig. A.1.

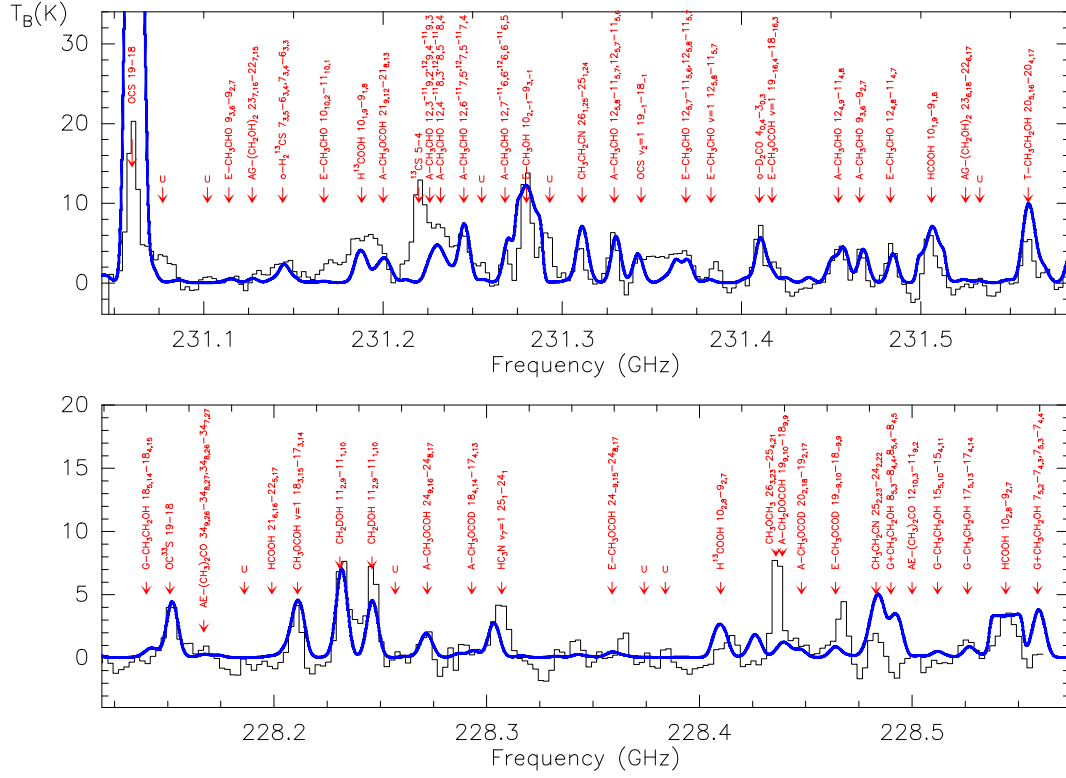


Fig. A.5. In blue, our synthetic spectrum superposed to the interferometric spectra published by FU05.

Table A.3. $\text{CH}_3\text{CN } \nu=0$ line parameters¹

N^2	Quantum numbers: up-low ³		ν (MHz)	E_u (K) ⁴	A_{ul} (s^{-1}) ⁵	S_{ij} ⁶	g_u ⁷	W (K km s^{-1}) ⁸	
1	12	11	220235.047	923.4	1.469E-04	1.92	25	1.95(1.95)	
2	12	10	220323.643	774.0	2.813E-04	3.67	25	4.73(1.38)	Blended with A- ¹³ CH ₃ OH
3	12	8	220475.814	517.6	5.125E-04	6.67	25	7.57(1.17)	
4	12	7	220539.328	410.6	6.091E-04	7.92	25	10.18(6.0)	
5	12	4	220679.287	175.1	8.223E-04	10.7	25	27.05(10.63)	
6	12	2	220730.259	89.4	9.000E-04	11.7	25	29.82(6.74)	
7	12	1	220743.008	68.0	9.195E-04	11.9	25	58.83(7.66)	
7	12	0	220747.259	68.9	9.259E-04	12.0	25		
8	12	6	220594.426	325.9	3.465E-04	9.00	50	19.37(6.83)	
9	12	3	220709.015	133.2	4.338E-04	11.	50	31.35(10.23)	

¹Exponential notation: $1.469\text{E-}04=1.469\times 10^{-4}$; ²Index to enumerate the line features in the spectrum (blended lines share the same index);

³Quantum numbers of the upper and lower levels of the transitions; ⁴Energy of the upper level; ⁵Einstein coefficient of spontaneous emission;

⁶Line strength defined as $|\mu_{ij}|^2 = S_{ij}\mu^2$ where μ is the dipole moment; ⁷Degeneracy of the upper level; ⁸Velocity integrated intensity

Table A.4. CH₃CN $\nu_8=1$ ($E_{vib}=525.17$ K) line parameters¹

N ²	Quantum numbers: up-low ³							ν (MHz)	E_{R_u} (K) ⁴	A_{ul} (s ⁻¹) ⁵	S_{ij} ⁶	g_u ⁷	W (K km s ⁻¹) ⁸		
1	12	8	1	12	11	8	1	11	221059.437	637.3	1.906E-03	24.6	25	3.63(1.57)	
1	12	8	1	13	11	8	1	12	221059.797	637.3	1.923E-03	26.8	27		
1	12	8	1	11	11	8	1	10	221059.828	637.3	1.904E-03	22.6	23		
2	12	-1	2	11	11	1	2	10	221199.140	68.1	1.705E-03	20.2	23	17.62(8.89)	Blended with CH ₃ OCH ₃
2	12	-1	2	12	11	1	2	11	221199.140	68.1	1.708E-03	22.0	25		
2	12	-1	2	13	11	1	2	12	221199.156	68.1	1.718E-03	23.9	27		
3	12	8	2	12	11	8	2	11	221209.781	423.9	9.551E-04	12.3	25	2.72(2.0)	
3	12	8	2	13	11	8	2	12	221210.140	423.9	9.634E-04	13.4	27		
3	12	8	2	11	11	8	2	10	221210.172	423.9	9.537E-04	11.3	23		
4	12	5	1	12	11	5	1	11	221252.937	319.3	2.844E-03	36.6	25	5.65(2.27)	
4	12	5	1	13	11	5	1	12	221252.937	319.3	2.863E-03	39.8	27		
4	12	5	1	11	11	5	1	10	221252.937	319.3	2.846E-03	33.7	23		
5	12	7	2	12	11	7	2	11	221265.547	330.5	2.269E-03	29.2	25	19.98(2.08)	Blended with CH ₃ OCHO
5	12	7	2	13	11	7	2	12	221265.547	330.5	2.288E-03	31.8	27		
5	12	7	2	11	11	7	2	10	221265.547	330.5	2.272E-03	26.9	23		
6	12	4	1	12	11	4	1	11	221299.875	241.8	1.532E-03	19.7	25	4.19(4.0)	Blended with CH ₃ OCHO
6	12	4	1	13	11	4	1	12	221299.875	241.8	1.540E-03	21.4	27		
6	12	4	1	11	11	4	1	10	221299.875	241.8	1.529E-03	18.1	23		
7	12	6	2	12	11	6	2	11	221311.953	251.2	1.291E-03	16.6	25	3.35(3.0)	
7	12	6	2	13	11	6	2	12	221311.953	251.2	1.303E-03	18.1	27		
7	12	6	2	11	11	6	2	10	221311.953	251.2	1.293E-03	15.3	23		
8	12	3	1	12	11	3	1	11	221338.218	178.5	1.618E-03	20.8	25	6.28(5.34)	Blended with aGg ⁻ -(CH ₂ OH) ₂
8	12	3	1	11	11	3	1	10	221338.218	178.5	1.615E-03	19.1	23		
8	12	3	1	13	11	3	1	12	221338.218	178.5	1.628E-03	22.6	27		
9	12	5	2	12	11	5	2	11	221350.375	186.1	1.424E-03	18.3	25	4.52(2.42)	
9	12	5	2	13	11	5	2	12	221350.375	186.1	1.433E-03	19.9	27		
9	12	5	2	11	11	5	2	10	221350.375	186.1	1.421E-03	16.8	23		
10	12	2	1	12	11	2	1	11	221367.672	129.5	3.354E-03	43.1	25	9.47(4.30)	Blended with A- ¹³ CH ₃ OH
10	12	2	1	11	11	2	1	10	221367.672	129.5	3.349E-03	39.6	23		
10	12	2	1	13	11	2	1	12	221367.672	129.5	3.379E-03	46.9	27		
11	12	4	2	12	11	4	2	11	221380.734	135.3	3.066E-03	39.4	25	16.77(1.81)	
11	12	4	2	11	11	4	2	10	221380.734	135.3	3.062E-03	36.2	23		
11	12	4	2	13	11	4	2	12	221380.734	135.3	3.084E-03	42.8	27		
12	12	0	2	11	11	0	2	10	221394.156	74.3	1.726E-03	20.4	23	18.99(1.15)	Blended with CH ₂ DOH
12	12	0	2	12	11	0	2	11	221394.156	74.3	1.728E-03	22.2	25		
12	12	0	2	13	11	0	2	12	221394.156	74.3	1.737E-03	24.1	27		
13	12	3	2	12	11	3	2	11	221403.812	98.7	1.619E-03	20.8	25	7.49(2.09)	Blended
13	12	3	2	11	11	3	2	10	221403.812	98.7	1.616E-03	19.1	23		
13	12	3	2	13	11	3	2	12	221403.812	98.7	1.629E-03	22.6	27		
14	12	2	2	12	11	2	2	11	221422.375	76.3	1.674E-03	21.5	25	15.61(7.19)	Blended with A- ¹³ CH ₃ OH
14	12	2	2	11	11	2	2	10	221422.375	76.3	1.676E-03	19.8	23		
14	12	2	2	13	11	2	2	12	221422.375	76.3	1.687E-03	23.4	27		
15	12	1	2	11	11	-1	2	10	221625.906	68.2	1.715E-03	20.2	23	9.94(2.67)	
15	12	1	2	12	11	-1	2	11	221625.906	68.2	1.718E-03	22.0	25		
15	12	1	2	13	11	-1	2	12	221625.906	68.2	1.728E-03	23.9	27		

¹Exponential notation: 1.469E-04=1.469×10⁻⁴; ²Index to enumerate the line features in the spectrum (blended lines share the same index);³Quantum numbers of the upper and lower levels of the transitions; ⁴Rotational energy of the upper level; ⁵Einstein coefficient of spontaneous emission; ⁶Line strength defined as $|\mu_{ij}|^2 = S_{ij}\mu^2$ where μ is the dipole moment; ⁷Degeneracy of the upper level; ⁸Velocity integrated intensity

Table A.5. CH₃OCHO line parameters¹

N	Quantum numbers: up-low						ν (MHz)	E_u (K)	A_{ul} (s ⁻¹)	S _{ij}	gu	W (K km s ⁻¹)	
									$\nu_t=0$				
1	17	3	14	16	3	13	218297.867	99.7	1.506E-04	16.4	35	10.21(8.88)	
2	17	4	13	16	4	12	220190.266	103.1	1.522E-04	16.1	35	18.05(2.43)	
3	33	5	28	33	5	29	220432.932	357.4	5.710E-06	1.16	67	9.36(3.90)	
4	17	-3	14	16	-3	13	218280.838	99.1	1.507E-04	43.6	35	9.96(2.90)	
5	17	-4	13	16	-4	12	220166.852	102.6	1.522E-04	42.9	35	13.96(0.37)	
6	18	13	6	17	13	5	221158.521	212.4	7.789E-05	22.9	37	10.09(3.66)	Blended with CH ₂ DOH
7	18	12	7	17	12	6	221280.890	195.8	9.063E-05	26.6	37	18.00(4.90)	Blended with ¹³ CH ₃ OH
8	18	-11	7	17	-11	6	221424.615	180.6	1.024E-04	30.0	37	16.19(4.35)	Blended with CH ₃ CN $\nu_t=8$
9	18	11	8	17	11	7	221445.622	180.6	1.025E-04	30.0	37	7.23(3.90)	
10	18	-10	8	17	-10	7	221649.374	166.7	1.134E-04	33.1	37	6.51(0.65)	
									$\nu_t=1$				
1	18	4	15	17	4	14	219704.898	299.5	1.507E-04	45.2	37	4.69(3.67)	
2	18	9	9	17	9	8	219764.090	342.7	1.198E-04	35.9	37	6.16(4.18)	
3	18	10	9	17	10	8	219822.160	355.1	1.105E-04	33.1	37	8.99(1.76)	
3	18	10	8	17	10	7	219822.161	355.1	1.105E-04	33.1	37		
4	18	9	10	17	9	9	220030.289	342.4	1.201E-04	35.9	37	7.60(7.00)	
4	18	9	9	17	9	8	220030.339	342.4	1.201E-04	35.9	37		
5	18	-10	9	17	-10	8	220307.810	354.8	1.115E-04	33.1	37	3.65(0.60)	
6	18	7	12	17	7	11	220913.784	321.3	1.375E-04	40.6	37	8.33(4.37)	
7	18	-8	11	17	-8	10	221111.015	330.7	1.308E-04	38.5	37	3.29 (2.88)	

¹Same notation as Table A.5.

Table A.6. CH₂DOH line parameters¹

N	Quantum numbers: up-low								ν (MHz)	E_u (K)	A_{ul} (s ⁻¹)	S _{ij}	gu	W (K km s ⁻¹)	
1	5	2	4	1	5	1	5	1	218316.390	58.7	1.818E-05	0.83	11	7.07(1.27)	
2	20	5	15	1	19	6	14	0	219206.135	557.6	2.977E-05	4.99	41	2.05(1.16)	
3	5	1	5	0	4	1	4	0	220071.805	35.8	2.614E-05	2.89	11	16.05(0.60)	Blended with CH ₃ OH
4	17	1	16	0	17	0	17	0	220552.586	335.9	7.545E-05	10.6	35	11.74(5.35)	
5	5	1	5	2	4	1	4	2	221273.004	54.7	3.371E-05	3.66	11	8.25(3.23)	
6	10	1	10	0	9	0	9	1	221391.766	120.2	5.674E-05	4.73	21	21.17(1.58)	Blended with CH ₃ CN $\nu_8=1$
7	20	2	18	2	20	1	19	2	221154.575	486.0	7.322E-05	12.0	41	13.20(2.10)	Blended with methyl formate
8	6	2	5	1	6	1	6	1	221178.153	71.6	2.067E-05	1.07	13	12.48(5.20)	Blended with HDCS

¹Same notation as Table A.5.

Table A.7. HNC line parameters¹

N	Quantum numbers: up-low						ν (MHz)	E_u (K)	A_{ul} (s ⁻¹)	S _{ii}	gu	W (K km s ⁻¹)
1	10	1	10	9	1	9	218981.009	101.1	1.462E-04	9.79	21	22.71(1.42)
2	10	3	8	9	3	7	219656.769	433.0	1.235E-04	8.19	21	10.68(1.48)
2	10	3	7	9	3	6	219656.771	433.0	1.235E-04	8.19	21	
3	10	2	9	9	2	8	219733.850	228.3	1.383E-04	9.17	21	27.10(1.89)
3	10	2	8	9	2	7	219737.193	228.3	1.383E-04	9.17	21	
4	10	0	10	9	0	9	219798.274	58.0	1.510E-04	1.00E+01a	21	27.85(4.74)
5	10	1	9	9	1	8	220584.751	101.5	1.494E-04	9.79E+00a	21	22.70(4.17)

¹Same notation as Table A.5.

Table A.8. aGg⁻-(CH₂OH)₂ line parameters¹

N	Quantum numbers: up-low								ν (MHz)	E_u (K)	A_{ul} (s ⁻¹)	S _{ij}	gu	W (K km s ⁻¹)	
1	22	4	19	0	21	4	18	1	218371.495	132.7	1.881E-04	145	405	3.07(3.00)	
2	22	15	7	0	21	15	6	1	218379.983	234.8	1.355E-04	81.4	315	2.21(0.17)	
2	22	15	8	0	21	15	7	1	218379.983	234.8	1.355E-04	105	405		
3	22	13	9	0	21	13	8	1	218574.680	207.3	1.652E-04	98.9	315	8.35(2.65)	Unidentified line?
3	22	13	10	0	21	13	9	1	218574.680	207.3	1.651E-04	127	405		
4	22	11	12	0	21	11	11	1	218872.112	183.8	1.911E-04	147	405	3.90(0.15)	
4	22	11	11	0	21	11	10	1	218872.112	183.8	1.911E-04	114	315		
5	22	10	13	0	21	10	12	1	219089.720	173.5	2.027E-04	155	405	5.06(0.49)	Blended with CH ₃ OCHO
5	22	10	12	0	21	10	11	1	219089.727	173.5	2.027E-04	121	315		
6	26	11	16	1	26	10	16	0	219384.910	232.5	5.221E-06	71.4	371	4.03 (0.05)	Well below the fit!
6	22	9	14	0	21	9	13	1	219385.177	164.3	2.136E-04	163	405		
6	26	11	15	1	26	10	17	0	219385.324	232.5	5.222E-06	91.7	477		
6	22	9	13	0	21	9	12	1	219385.425	164.3	2.136E-04	127	315		
7	22	1	21	1	21	1	20	0	219580.671	122.2	2.568E-04	195	405	12.63(0.56)	Blended with CH ₃ OCHO
9	20	4	16	1	19	4	15	0	219764.925	114.4	2.453E-04	169	369	9.50(0.60)	Blended with CH ₃ OCHO
9	21	4	18	1	20	4	17	0	221007.823	122.6	2.657E-04	189	387	5.67(0.28)	
10	22	6	17	0	21	6	16	1	221038.799	142.6	2.395E-04	178	405	3.77(0.42)	
11	22	5	18	0	21	5	17	1	221100.315	137.4	2.368E-04	176	405	3.39(0.26)	
12	23	3	21	0	22	3	20	1	221338.974	138.4	2.717E-04	164	329	7.19(0.075)*	Blended with CH ₃ CN $\nu_8=1$

¹Same notation as Table A.5.

*In Fig. 2, we have subtracted the CH₃CN $\nu_8=1$ contribution that accounts for ~50% of the flux